Research Paper

GEOSPHERE

GEOSPHERE

https://doi.org/10.1130/GES02696.1

12 figures; 1 table; 1 set of supplemental files

CORRESPONDENCE:
renaud.soucy_la_roche@ete.inrs.ca

CITATION: Soucy La Roche, R., Zagorevski, A., Joyce, N.L., and Crowley, J.L., 2024, Paleozoic evolution of the Yukon-Tanana terrane of the North American Cordillera, NW British Columbia: Geosphere, https://doi.org/10.1130/GES02696.1.

Science Editor: Christopher J. Spencer
Associate Editor: Mark Holland

Received 22 June 2023
Revision received 8 November 2023
Accepted 20 December 2023

Published online 15 February 2024

Paleozoic evolution of the Yukon-Tanana terrane of the North American Cordillera, NW British Columbia

R. Soucy La Roche[1,2], A. Zagorevski[2], N.L. Joyce[2], and J.L. Crowley[3]

[1]Centre Eau Terre Environnement, Institut National de la Recherche Scientifique, 490 rue de la Couronne, Québec, Québec G1K9A9, Canada
[2]Geological Survey of Canada, Natural Resources Canada, 601 Booth Street, Ottawa, Ontario K1A 0E8, Canada
[3]Department of Geoscience, Boise State University, 1910 University Drive, Boise, Idaho 83725-1535, USA

ABSTRACT

The origins and primary relationships between tectono-stratigraphic units are fundamental to the terrane concept in accretionary orogens, but they are challenging to assess in metamorphic terranes. In NW British Columbia, three tectonically bounded metamorphic suites of the Yukon-Tanana terrane formed in distinct tectonic settings, based on high-spatial-resolution geochronology and immobile trace-element geochemistry. The Florence Range suite comprises late Neoproterozoic or younger to pre–latest Devonian metasedimentary rocks derived from continental crust, 360 ± 4 Ma calc-alkaline intermediate orthogneiss, and 357 ± 4 Ma amphibolite with oceanic-island basalt composition, consistent with rifting of a continental margin. The detrital signature is dominated by late Mesoproterozoic zircon, which indicates different sources than other parts of the Yukon-Tanana terrane. The Boundary Ranges suite comprises pre–Late Devonian metasedimentary rocks derived in part from a mafic source, amphibolite derived from subduction-zone metasomatized mantle, and 369 ± 4 Ma to 367 ± 7 Ma calc-alkaline felsic to intermediate orthogneiss. The Whitewater suite comprises meta-chert, graphite-rich metapelite, and amphibolite with back-arc basin basalt composition consistent with an anoxic basin near a volcanic source. Our data indicate that the Florence Range and Boundary Ranges suites were separate until at least the Early Mississippian and may have formed a composite terrane since the Permian, whereas the relationship with the Whitewater suite is uncertain. We compare the Paleozoic evolution of the Yukon-Tanana terrane in NW British Columbia with several modern analogues in the west and southwest Pacific Ocean.

INTRODUCTION

Accretionary orogens are major sites of continental growth and mineralization as well as consumption and reworking of continental crust (Condie et al., 2007; Cawood et al., 2009). Accretionary processes and tectonic models of accretionary orogens depend on a wide range of combinations of diverse parameters including the nature, age, and physical properties of the convergent elements, preexisting structures, convergence velocity and direction, and the time scale of the orogeny (Brown et al., 2011). Many of these parameters are difficult to constrain in ancient accretionary orogens, but the nature and age of the converging elements (e.g., continental margin, arcs, back-arcs, oceanic plateaus, etc.) are generally well preserved in the rock record and are foundational to the development of tectonic models.

The North American Cordillera is a classic example of a Phanerozoic accretionary orogen that had a significant impact on current understanding of continental growth and subduction processes (Coney et al., 1980; Monger et al., 1982; Saleeby, 1983; Colpron et al., 2007; Monger and Gibson, 2019). It is divided into terranes that were originally defined by apparent internal homogeneity and continuity of stratigraphy, tectonic style, and history (Coney et al., 1980). The birth of the northern Cordilleran orogen is generally ascribed to the early Mesozoic (e.g., Colpron et al., 2015, 2022), yet the assembly of the orogen was strongly influenced by the Paleozoic evolution of the Laurentian margin and the paleogeographic position of the various terranes (Parsons et al., 2022). Advances in analytical methods, such as geochronology and geochemistry, and their widespread application in the northern Cordillera provided better constraints on the origin and evolution of terrane constituents and highlighted the heterogeneous nature of several terranes. Indeed, the tectonic context in which terrane-forming units form varies with time, but the tectonic origin of coeval rocks can also vary with space. In some cases, spatial variations have been ascribed to facies changes in an overall coherent tectonic setting (e.g., Colpron et al., 2006a, 2007; Colpron and Nelson, 2011). In other cases, rocks formed and evolved as independent tectonic blocks until they were merged into composite terranes during a collision outboard of Laurentia or during accretion to its margin (e.g., the Cache Creek and Atlin terranes—Zagorevski et al., 2021; the composite Yukon-Tanana terrane—van Staal et al., 2018; Parsons et al., 2018, 2019, 2022; Ryan et al., 2021). In some terranes, such as the Yukon-Tanana terrane, the proper identification of protoliths and the evaluation of tectono-stratigraphic relationships are hindered by polyphase metamorphism and deformation, which destroyed primary textures, contacts, and any fossils sedimentary units may have contained. Combined use of high-spatial-resolution geochronology that can identify protolith and metamorphic ages

Renaud Soucy La Roche https://orcid.org/0000-0002-6907-2841; Alexandre Zagorevski https://orcid.org/0000-0002-2314-4811; Nancy Joyce https://orcid.org/0000-0002-9103-0728; James Crowley https://orcid.org/0000-0001-5069-0773

along with immobile trace-element geochemistry can help to resolve the origin and primary relationships between the various tectono-stratigraphic units.

This study targeted several suites of medium- to high-metamorphic-grade rocks in NW British Columbia that were previously correlated to the Yukon-Tanana terrane (e.g., Mihalynuk et al., 1999). We analyzed their geochemical composition in combination with U-Pb geochronology on detrital zircon from metasedimentary units and igneous zircon from meta-igneous units. Based on these data, we interpreted the tectonic setting of formation and evolution of these metamorphic rocks. We demonstrate that these metamorphic suites formed in distinct, but possibly genetically linked tectonic settings. Their subsequent amalgamation resulted in the formation of the southwest portion of the composite Yukon-Tanana terrane. Several Paleozoic tectonic scenarios compatible with published and new data are illustrated with modern analogues in the west and southwest Pacific Ocean.

GEOLOGICAL SETTING

The Intermontane superterrane of the northern Cordillera is composed of several terranes that were derived from the western margin of Laurentia or formed within its vicinity (Yukon-Tanana, Stikine, Quesnellia, Cache Creek, Atlin, and Slide Mountain terranes; Colpron et al., 2006a, 2007; Zagorevski et al., 2021). The Yukon-Tanana terrane is the most spatially extensive of the Intermontane terranes in eastern Alaska, central Yukon, and NW British Columbia (Fig. 1; Mortensen, 1992). It has a complex and protracted Paleozoic to early Mesozoic history. The basement of the Yukon-Tanana terrane, represented by the Late Devonian and older siliciclastic rocks of the Snowcap assemblage in Yukon, initially formed along the Laurentian margin and rifted away during the Late Devonian (Tempelman-Kluit, 1979; Nelson et al., 2006; Colpron et al., 2006a, 2006b, 2007; Piercey and Colpron, 2009). The Snowcap assemblage is intruded by magmatic rocks and overlain by associated volcaniclastic rocks that formed during six Paleozoic magmatic cycles (e.g., Piercey et al., 2006; Nelson et al., 2006). The first four magmatic cycles (Ecstall cycle at 390–365 Ma, Finlayson cycle at 365–357 Ma, Wolverine cycle at 357–342 Ma, and Little Salmon cycle at 342–314 Ma) are characterized by variable compositions (felsic and mafic) and geochemical signatures, including mafic rocks with normal mid-ocean-ridge basalt (N-MORB), enriched MORB (E-MORB), oceanic-island basalt (OIB), island-arc tholeiite (IAT), and calk-alkaline basalt (CAB) characteristics. Units with arc signature are generally more common in the western part of the Yukon-Tanana terrane, whereas units with MORB or OIB compositions are more common in the eastern part. This spatial distribution was attributed to variations in an arc (west)–back-arc (east) system (Piercey et al., 2006; Nelson et al., 2006). Local spatial association of E-MORB, OIB, and IAT signatures has been attributed to intra-arc rifting events (e.g., Simard et al., 2007). Alternatively, this spatial association could be the result of broad lithospheric extension (Zagorevski and van Staal, 2021). The younger, Pennsylvanian to early Permian Klinkit cycle (314–269 Ma) is dominated by mafic to andesitic volcanic rocks, with

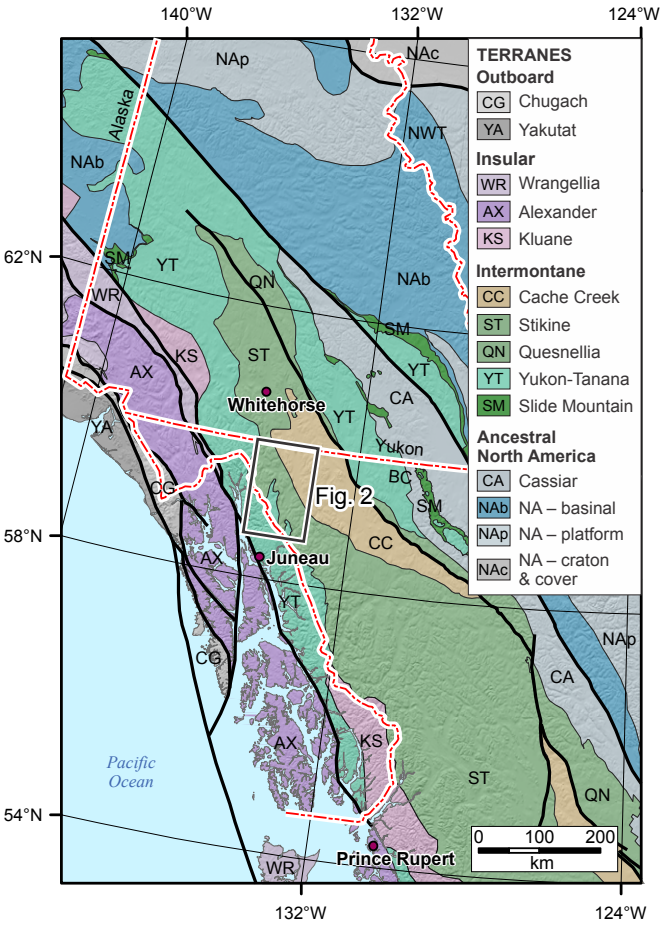

Figure 1. Map of the Northern Cordilleran terranes after Colpron and Nelson (2011) with location of study area. BC—British Columbia; NA—North America; NWT—Northwest Territories.

rare cogenetic plutons, and it is characterized by an intra-oceanic calc-alkaline to tholeiitic character, interpreted to represent a volcanic arc built on strongly attenuated lithosphere (Piercey et al., 2006; Nelson et al., 2006). The spatially limited middle to late Permian Klondike cycle (269–253 Ma) marks the final pulse of calc-alkaline magmatism in an arc (Piercey et al., 2006; Nelson et al., 2006) or a continental rift setting (Canil et al., 2003; Johnston et al., 2007; Zagorevski and van Staal, 2021).

The Yukon-Tanana terrane records ~300 m.y. of episodic eclogite-facies, Barrovian and low-pressure contact metamorphism (see review in Soucy La Roche

et al., 2022a). Metamorphic events include Early Mississippian blueschist- to eclogite-facies (Erdmer et al., 1998; Devine et al., 2006), middle to late Permian eclogite- and greenschist- to lower-amphibolite-facies (Creaser et al., 1997a; Philippot et al., 2001; Beranek and Mortensen, 2011; Petrie et al., 2016; Soucy La Roche et al., 2022a), Middle Triassic pyroxene hornfels–facies (Berman et al., 2007; Gaidies et al., 2021), Early Jurassic upper-amphibolite-facies (Berman et al., 2007; Dyer, 2020; Gaidies et al., 2021; Soucy La Roche et al., 2022a), Middle Jurassic to Early Cretaceous lower- to middle-amphibolite-facies and hornblende hornfels–facies (Berman et al., 2007; Staples et al., 2014; Soucy La Roche et al., 2022a), and Late Cretaceous middle-amphibolite-facies metamorphism (Vice et al., 2020).

METAMORPHIC SUITES IN NW BRITISH COLUMBIA

In NW British Columbia, polydeformed amphibolite-facies metamorphic rocks are exposed west of the Llewellyn fault, a subvertical, brittle-ductile deformation zone that was episodically active in the Cretaceous and Eocene (Ootes et al., 2018, 2019). This fault separates the amphibolite-facies rocks from zeolite- to greenschist-facies units of the Stikine terrane (Greenwood et al., 1991; Mihalynuk et al., 1999; Logan et al., 2000). Amphibolite-facies rocks have been subdivided into the Florence Range, the Boundary Ranges, and the Whitewater metamorphic suites (Fig. 2; Mihalynuk and Rouse, 1988; Mihalynuk and Mountjoy, 1990; Currie, 1990, 1991; Mihalynuk et al., 1989, 1994, 1999; Soucy La Roche et al., 2022a). The Florence and Boundary Ranges suites are exposed west of Atlin and Tagish Lakes, whereas the Whitewater suite is exposed to the south (Fig. 2). The Florence Range suite is separated from the Boundary Ranges suite by the Wann River shear zone, which is interpreted to have been active between 185 Ma and 170 Ma (Currie, 1992a, 1994; Currie and Parrish, 1993; Soucy La Roche et al., 2022a), although this shear zone records polyphase deformation and might have been active before 185 Ma (Soucy La Roche et al., 2022b). The Whitewater suite is separated from the Boundary Ranges suite by unnamed faults (Mihalynuk et al., 1994).

The Florence Range suite (Currie, 1990, 1991) comprises polymetamorphic upper-amphibolite-facies metasedimentary units including biotite-muscovite quartzofeldspathic schist and gneiss and minor layers of metapelite, quartzite, marble, and calc-silicate gneiss. These units were interpreted to represent a metamorphosed continental-margin sedimentary sequence (Currie, 1994) included in the Tracy Arm terrane (Coney et al., 1980) or Nisling terrane (Wheeler et al., 1991), and subsequently correlated to the Snowcap assemblage of the Yukon-Tanana terrane in Yukon (Nelson et al., 2006). The Florence Range suite includes rare felsic to intermediate orthogneiss and amphibolite (Currie, 1994). Dated meta-igneous rocks are restricted to the Wann River shear zone and include the Permian Wann River gneiss (270 ± 5 Ma igneous crystallization age, U-Pb zircon; Currie, 1992a), a pervasively sheared hornblende-plagioclase orthogneiss that is interlayered at the map and outcrop scales with metasedimentary schist and gneiss of the Florence Range suite (Currie and Parrish, 1997). This unit was interpreted as a structurally interleaved metavolcanic unit related to the Boundary Ranges suite by Currie and Parrish (1997); however, the Wann River gneiss may instead represent strongly sheared metaplutonic rocks, based on field observations (Zagorevski et al., 2018). The Florence Range suite was metamorphosed to at least the kyanite zone during the Permian to Middle Triassic (270–240 Ma), to the suprasolidus sillimanite and K-feldspar zone during the Early Jurassic (195–170 Ma), and finally to the andalusite and cordierite zone during late Early Cretaceous contact metamorphism (U-Pb monazite and xenotime—Soucy La Roche et al., 2022a; Lu-Hf garnet—Dyer, 2020).

The Boundary Ranges suite (Mihalynuk and Rouse, 1988; Mihalynuk et al., 1989; Mihalynuk and Mountjoy, 1990) comprises lower-amphibolite-facies metasedimentary and meta-igneous rocks, including muscovite-biotite ± garnet quartzofeldspathic schist, chlorite-actinolite ± garnet schist, and rare graphitic schist and marble. The origin of these Boundary Ranges units is poorly understood. Protoliths have been interpreted to represent island-arc volcanosedimentary rocks correlative to the Yukon-Tanana terrane (Mihalynuk et al., 1999) or to the basement of the Stikine terrane (Stikine assemblage; Currie and Parrish, 1997). The Boundary Ranges suite contains felsic orthogneiss that yielded variably discordant Late Devonian to Early Mississippian U-Pb zircon dates (Currie and Parrish, 1997). Available peak metamorphic conditions reached 550–600 °C and 0.6–0.8 MPa at 200–190 Ma (Lu-Hf garnet; Dyer, 2020), but the polydeformed nature of the Boundary Ranges suite (Currie and Parrish, 1993, 1997; Currie, 1994) indicates that the Boundary Ranges suite was affected by multiple tectonic and possibly metamorphic episodes.

The Whitewater suite (Mihalynuk et al., 1994) comprises lower-amphibolite-facies quartzite, amphibolite, and graphitic metapelite with minor marble, quartzofeldspathic schist, felsic orthogneiss, and meta-peridotite. This suite has been correlated with the Boundary Ranges suite and with parts of the Yukon-Tanana terrane in Yukon based on the association of metasedimentary and metavolcanic rocks interpreted to have formed on a continental margin next to a volcanic arc (Mihalynuk et al., 1994). The Whitewater suite is polydeformed, and the timing of peak metamorphism is not constrained, but it has been inferred to be Early to Middle Jurassic (Mihalynuk et al., 1994).

The three metamorphic suites are intruded by the variably deformed Early Jurassic Tagish Lake suite (187 ± 1.1 Ma and 180.9 ± 3.1 Ma igneous crystallization ages, U-Pb zircon; Currie, 1992a, 1994, Currie and Parrish, 1997), although its extent is limited in the Whitewater suite, and it has been recognized in the Florence Ranges suite only within the Wann River shear zone. Cretaceous to Eocene felsic to intermediate plutonic and volcanic rocks of the Coast belt and Sloko suites form an overlap assemblage in all metamorphic suites (130–55 Ma igneous crystallization ages; Currie, 1992b; Mihalynuk et al., 1999, and references therein).

U-Pb ZIRCON GEOCHRONOLOGY

U-Pb zircon geochronology was used to constrain the maximum age of deposition and provenance of sedimentary protoliths and the crystallization

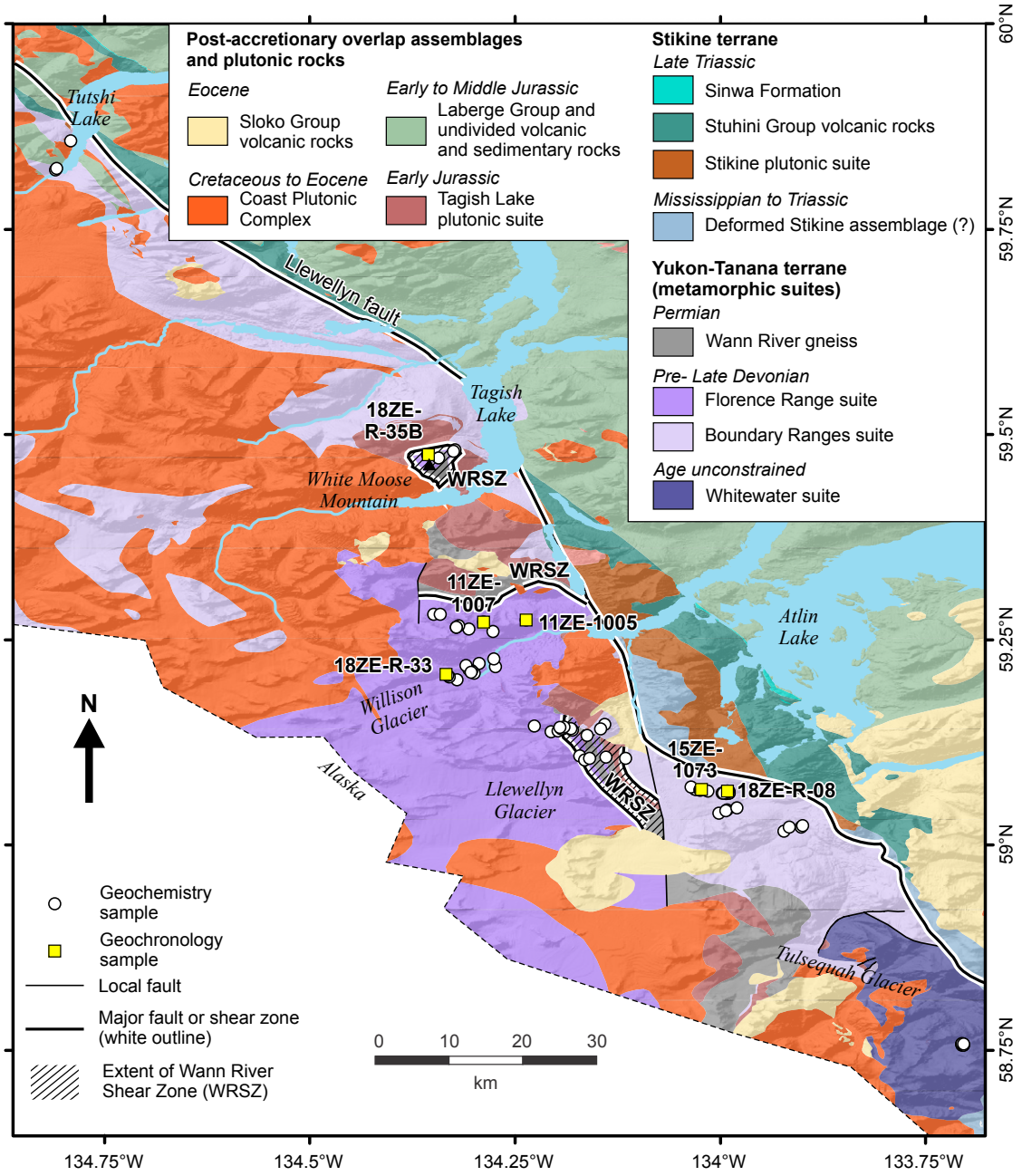

Figure 2. Simplified geological map of the Atlin Lake area modified from Cui et al. (2017) and based on Mihalynuk et al. (1999), with the locations of samples in this study. Samples used for geochronology are labeled with their sample number. Topography is displayed with a hillshade digital elevation model (Natural Resources Canada, 2016). Hatching indicates the extent of the Wann River shear zone (WRSZ; Soucy La Roche et al., 2022a).

age of igneous protoliths, and it provides constraints on regional metamorphism. Results from two quartzofeldspathic schist samples from the Florence Range suite are presented, one of which was previously reported in Kellett and Iraheta Muniz (2019). One orthogneiss sample and one amphibolite sample from the Florence Range suite and two orthogneiss samples from the Boundary Ranges suite were also analyzed. Thirteen metasedimentary samples from the Boundary Ranges suite were scanned with the AZtec Feature tool on a scanning electron microscope (SEM; see details in Soucy La Roche et al., 2022a), but they did not contain zircon sufficiently large to be analyzed. Whitewater suite metasedimentary rocks failed to yield any zircon. All results are reported in Tables S1 and S2, whereas backscattered electron (BSE) and cathodoluminescence (CL) images of all grains are included in Figure S1.[1] Additional concordia diagrams are presented in Figure S2. Global positioning system (GPS) coordinates of samples and a summary of results are reported in Table 1.

Analytical Methods

Zircon grains were separated using standard techniques, mounted in epoxy, and polished until their centers were exposed. Zircon grains were imaged in BSE mode and CL mode except for sample 18ZE-R-08 (CL only). Zircon from samples 11ZE-1005, 15ZE-1073, 18ZE-R-35B, and 18ZE-R-33 was analyzed by sensitive high-resolution ion microprobe (SHRIMP) at the Geological Survey of Canada following analytical procedures of Stern (1997), with standards and U-Pb calibration methods following Stern and Amelin (2003). Zircon from sample 18ZE-R-08 was analyzed by laser ablation–inductively coupled plasma–mass spectrometry (LA-ICP-MS) using a ThermoElectron X-Series II quadrupole ICP-MS and New Wave Research UP-213 Nd:YAG UV (213 nm) laser-ablation system at Boise State University, using in-house analytical protocols, standard materials, and data reduction software. Additional details about zircon separation, imaging, standards, secondary reference materials, and data processing are available in Text S1.

Several precautions were taken to ensure that individual dates represent unique and homogeneous age domains. CL and BSE images were used to identify analyses that may have sampled multiple chemical or age domains, inclusions, microfractures, or matrix material. SHRIMP analyses with U >2000 ppm (considered to be above the calibration range) or probability of concordance <0.05 were not included in weighted mean age calculations. LA-ICP-MS results with anomalous trace-element compositions (e.g., Ti or P) indicative of ablation of an inclusion and those that appeared to be contaminated by common Pb based on the mass ^{204}Pb above baseline were rejected from interpretations.

Isoplot v. 4.15 (Ludwig, 2003a) was used to calculate weighted averages and to generate concordia plots and weighted average date plots. AgeDisplay (Sircombe, 2004) was used to generate combined histogram and probability density plots of individual samples, and NORMALIZED PROB PLOT (Arizona LaserChron Center; www.laserchron.org) was used to generate stacked normalized probability density plots. Age interpretations were based on ^{206}Pb/^{238}U dates for dates younger than 1 Ga and ^{207}Pb/^{206}U dates for dates older than 1 Ga. Uncertainties on individual dates and weighted averages are reported in the text at 2σ. Uncertainties on weighted averages include the standard calibration error. An evaluation of the long-term reproducibility of the ^{206}Pb/^{238}U age of secondary standard 9910 indicated that the minimum reproducibility precision of SHRIMP weighted average results is 1% (2σ, based on 51 analytical sessions). In cases where the precision of the weighted average age calculation for individual samples fell below this threshold, the weighted average 2σ uncertainty was augmented to 1%. Similarly, uncertainties on weighted average LA-ICP-MS dates are minimally 2%, consistent with the long-term reproducibility precision and accuracy of secondary reference materials analyzed with LA-ICP-MS (e.g., Horstwood et al., 2016). We use the terms "date" and "age" to refer to results and their interpretation with a geological significance, respectively.

[1]Supplemental Material. Table S1: Sensitive high-resolution ion microprobe (SHRIMP) U-Pb geochronology results. Table S2: Laser ablation–inductively coupled plasma–mass spectrometry (LA-ICP-MS) U-Pb geochronology results. Table S3: Geochemistry results. Figure S1: Backscattered electron and cathodoluminescence images of zircon. Figure S2: Concordia diagrams. Figure S3: Supplemental geochemical diagrams. Text S1: Detailed geochronological methods. Please visit https://doi.org/10.1130/GEOS.S.25050536 to access the supplemental material, and contact editing@geosociety.org with any questions.

TABLE 1. SAMPLE LOCATIONS AND SUMMARY OF GEOCHRONOLOGY RESULTS FROM METAMORPHIC SUITES, NW BRITISH COLUMBIA

Sample	Metamorphic suite	Rock type	Latitude (°N)	Longitude (°W)	Maximum age of deposition (Ma)	Igneous crystallization age (Ma)	Metamorphic age (Ma)
11ZE-1005	Florence Range	Quartzofeldspathic schist	59.274450	134.236400	704 ± 16	N.A.	239 ± 6
11ZE-1007	Florence Range	Quartzofeldspathic schist	59.272110	134.288350	660 ± 11	N.A.	183 ± 5
15ZE-1073	Boundary Ranges	Leucocratic orthogneiss	59.068136	134.024750	N.A.	369 ± 4	288 ± 7
18ZE-R-08	Boundary Ranges	Leucocratic orthogneiss	59.065880	133.991459	N.A.	367 ± 7	None
18ZE-R-35B	Florence Range	Mesocratic orthogneiss	59.475991	134.356817	N.A.	360 ± 4	187 ± 2
18ZE-R-33	Florence Range	Amphibolite	59.205092	134.330529	N.A.	357 ± 4	Early Jurassic

Notes: North American Datum (NAD) 1983 geodetic datum. N.A.—not applicable.

Sample Descriptions, Results, and Interpretations of Dates

Samples 11ZE-1005 and 11ZE-1007

Samples 18ZE-1005 and 18ZE-1007 are Florence Range suite quartz-plagioclase-biotite-muscovite (Qz-Pl-Bt-Ms) ± garnet (Grt) schists collected ~3 km apart along the ridge north of Willison Creek (Fig. 2). They likely represent different quartzofeldspathic schist layers separated by more quartzofeldspathic schist, marble, quartzite, and metapelite.

Zircon is similar in both samples. It is abundant, 50–150 µm long, and equant to slightly elongate (1:1–2:1) and has rounded edges (Fig. 3A). Variable zoning patterns include oscillatory, sector, and patchy zoning. Zoning is commonly truncated at grain edges. Rare, thin (<30 µm) CL-bright and CL-dark rims completely surround grains or form faceted overgrowths at grain tips.

Zircon from sample 11ZE-1005 yielded concordant dates ranging from 1675 ± 36 Ma to 704 ± 16 Ma (Fig. 3B). Most dates form two peaks at 1.2–1.0 Ga and 1.5–1.3 Ga. Dates older than 1.5 Ga are almost all discordant. Zircon from sample 11ZE-1007 yielded concordant dates ranging from 2728 ± 28 Ma to 183 ± 5 Ma (Fig. 3B). Most dates are scattered between 1.5 Ga and 1.0 Ga (peaks at ca. 1.45 Ga, 1.35 Ga, 1.2 Ga, and 1.15 Ga) and between 1.8 Ga and 1.7 Ga. A few other zircon grains yielded Early Jurassic, late Neoproterozoic, and Archean dates.

To identify the youngest detrital zircons, postdeposition metamorphic zircon must be recognized. Early Jurassic upper-amphibolite-facies metamorphism is documented in the area (Soucy La Roche et al., 2022a; Dyer, 2020); therefore, the youngest zircon in sample 11ZE-1007 (183 ± 5 Ma) is likely metamorphic. In sample 11ZE-1005, a slightly discordant 239 ± 6 Ma analysis could have resulted from Permian–Triassic metamorphism (e.g., Soucy La Roche et al., 2022a). The maximum age of deposition is constrained by the age of the youngest

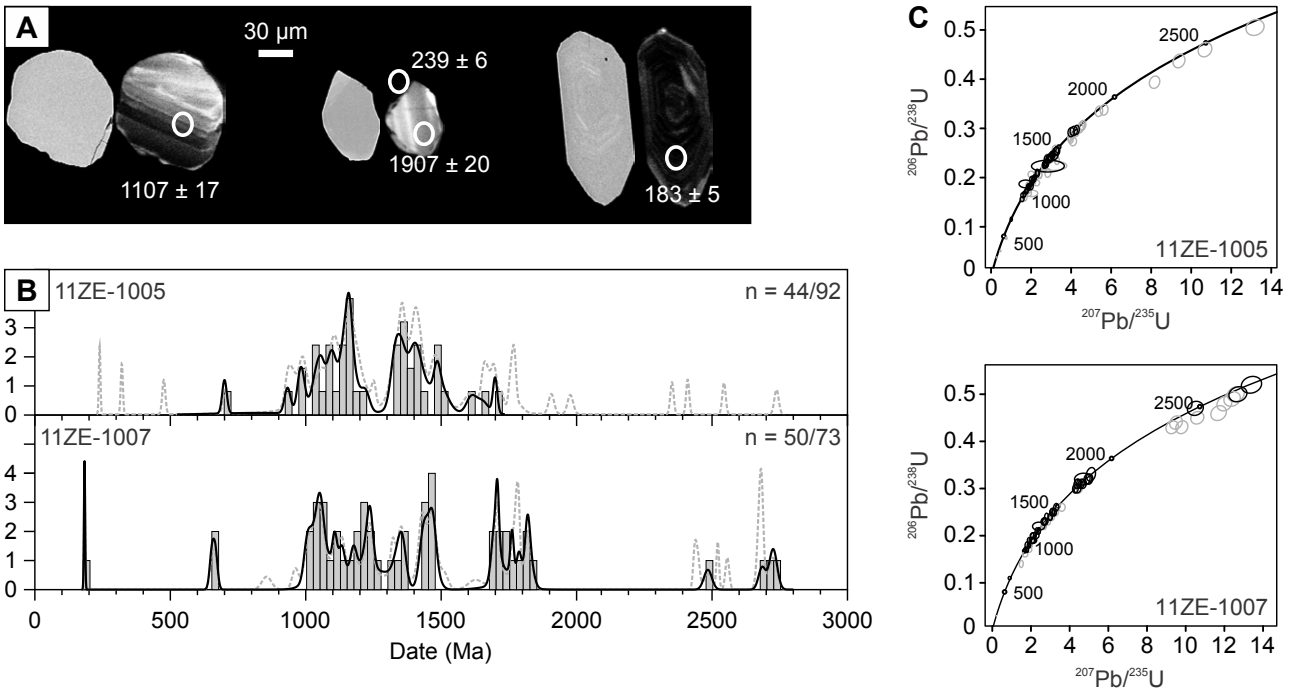

Figure 3. Metasedimentary rocks analyzed for U-Pb zircon geochronology. (A) Backscattered-electron (left) and cathodoluminescence (CL; right) images of rounded detrital zircon with truncated oscillatory zoning, Triassic CL-dark metamorphic overgrowth on detrital zircon, and Early Jurassic metamorphic zircon. Dates are in Ma. (B) Probability density plots of U-Pb dates. The black curve includes only analyses with probability of concordance >0.05; the dashed gray curve includes all analyses. Histogram includes only concordant data in 25 m.y. bins. Dates younger than 1 Ga and older than 1 Ga are $^{206}Pb/^{238}U$ and $^{207}Pb/^{206}U$ dates, respectively. (C) Concordia diagrams. Error ellipses are 2σ. Gray ellipses have a probability of concordance <0.05. Dates for sample 11ZE-1005 are from Kellett and Iraheta Muniz (2019).

concordant analysis on detrital zircon (704 ± 16 Ma) in sample 11ZE-1005, and by the youngest and second youngest concordant analyses on detrital zircon (652 ± 16 Ma and 664 ± 14 Ma) in sample 11ZE-1007.

Sample 15ZE-1073

Sample 15ZE-1073 is a well-foliated, fine-grained, leucocratic Pl–Qz–K-feldspar–white mica–Bt–epidote–chlorite–calcite (Pl-Qz-Kfs-WM-Bt-Ep-Chl-Cal) orthogneiss exposed at the toe of Llewellyn Glacier (Fig. 2). The relationship between this unit and adjacent units from the Boundary Ranges suite is difficult to interpret because the rarely exposed contacts are parallel to the foliation (Fig. 4A). Although unambiguous crosscutting relationships were not observed, the orthogneiss is in contact with different layers of schist with variable composition, indicating that it may have crosscut host lithological units, consistent with a metaplutonic origin.

Zircon is abundant, 75–500 µm long, and equant to elongate (1:1–5:1) and displays complex zoning patterns consistent with multiple generations of zircon (Fig. 4B). The dominant population is composed of euhedral to subhedral, oscillatory zoned and, more rarely, patchy or sector zoned zircon that yielded dates ranging from 382 ± 9 Ma to 350 ± 19 Ma. Th/U ranged from 0.38 to 0.96 with an average of 0.56. A second generation of zircon forms thin (5–25 µm), incomplete, CL-bright homogeneous to oscillatory zoned overgrowths. Most analyses on these rims were aborted or excluded from interpretations because they clearly overlapped the core and the rim due to the large spot size (16 µm) or for various analytical issues (see Table S1). These rims were specifically targeted during a second round of analysis with a smaller, 9 µm spot size and yielded five lower-precision concordant dates on four zircon rims ranging from 297 ± 29 Ma to 282 ± 12 Ma. The Th/U of the overgrowths ranged from 0.33 to 0.58 with an average of 0.44.

We interpret the Late Devonian population to be magmatic based on its euhedral to subhedral morphology, oscillatory zoning, and high Th/U typical of magmatic zircon (Rubatto and Gebauer, 2000; Corfu et al., 2003; Hoskin and Schaltegger, 2003; Rubatto, 2017). Analyses from this group of zircon gave a weighted average date of 369 ± 4 Ma (mean squared weighted deviation [MSWD] = 3.0; probability of fit [*P*] = 0.00; number of analyses in the weighted average [*n*] = 30) with excess scatter that cannot be attributed to analytical uncertainties (Wendt and Carl, 1991; Ludwig, 2003b). This scatter in dates could indicate protracted (re-)crystallization over a time range, Pb loss resulting in younger dates, or inheritance or an amount of common ^{204}Pb too small to be measured, resulting in older dates, or a combination of these factors. Unequivocal outliers could not be identified based on texture or chemical composition at the upper or lower end of the date distribution. We therefore interpret the 369 ± 4 Ma as the best estimate of the magmatic crystallization age of the orthogneiss protolith despite the minor scatter (Figs. 4C and 4D).

The scarcity and morphology of the Permian overgrowths are characteristic of metamorphic zircon (Rubatto and Gebauer, 2000; Corfu et al., 2003; Hoskin and Schaltegger, 2003; Rubatto, 2017) and indicate that a metamorphic event occurred in the Boundary Ranges suite at 288 ± 7 Ma (MSWD = 0.67; *P* = 0.61; *n* = 5) (Fig. 4C).

Sample 18ZE-R-08

Sample 18ZE-R-08 is a well-foliated, fine-grained, leucocratic Qz-Pl-WM-Kfs-Chl-Bt-Grt-Ep orthogneiss exposed at the toe of Llewellyn Glacier (Figs. 2 and 4E). The relationship between this unit and adjacent units from the Boundary Ranges suite is difficult to interpret because the rare exposed contacts are parallel to the foliation.

Zircon is rare, <100 µm long, equant to slightly elongate (1:1–2:1) and euhedral, and displays sector and more rarely oscillatory zoning (Fig. 4F). Rare discrete (xenocrystic?) cores are visible, but they are too small (<30 µm) to be analyzed with LA-ICP-MS. Zircon yielded dates ranging from 384 ± 10 Ma to 351 ± 5 Ma. Th/U ranged from 0.35 to 0.94 with an average of 0.58.

The high MSWD and null *P* of the weighted average date (366 ± 7 Ma; MSWD = 4.7; *P* = 0.00; *n* = 21) indicate that there is excess scatter that cannot be attributed to analytical uncertainties (Wendt and Carl, 1991; Ludwig, 2003b). This scatter in dates could be caused by protracted (re-)crystallization over a time range, Pb loss resulting in younger dates for the youngest analyses, inheritance or an amount of common ^{204}Pb too small to be measured, and resulting in older dates for the oldest analyses, or a combination of these factors. Excluding the two youngest dates that may have been affected by Pb loss, and the four oldest dates from zircon, which displayed clear oscillatory zoning and may not be autocrysts (in the sense of Miller et al., 2007), resulted in a statistically homogeneous population (e.g., Wendt and Carl, 1991; Ludwig, 2003b) with an equivalent weighted average date of 367 ± 7 Ma (MSWD = 0.93; *P* = 0.52; *n* = 15), which we interpret as the magmatic crystallization age of the orthogneiss protolith (Figs. 4G and 4H).

Sample 18ZE-R-35B

Sample 18ZE-R-35B is a well-foliated, medium-grained, mesocratic Florence Range suite Qz-Pl-Bt-Ep-Kfs-Chl orthogneiss located within the Wann River shear zone at White Moose Mountain (Figs. 2 and 4I). This orthogneiss unit is several tens of meters thick, and the contact with adjacent units was not observed.

Zircon is abundant, 100–300 µm long, and equant to elongate (1:1–4:1) and displays complex zoning patterns consistent with multiple generations of zircon (Fig. 4J). One xenocrystic core yielded a discordant 1735 ± 64 Ma date. The dominant population is composed of euhedral oscillatory zoned zircon that yielded dates ranging from 366 ± 8 Ma to 340 ± 8 Ma. Th/U ranged from 0.28 to 0.67 with an average of 0.41. Two zircon grains displayed oscillatory and patchy zoning and were dated at 264 ± 6 Ma (Th/U = 0.27) and 297 ± 8 Ma

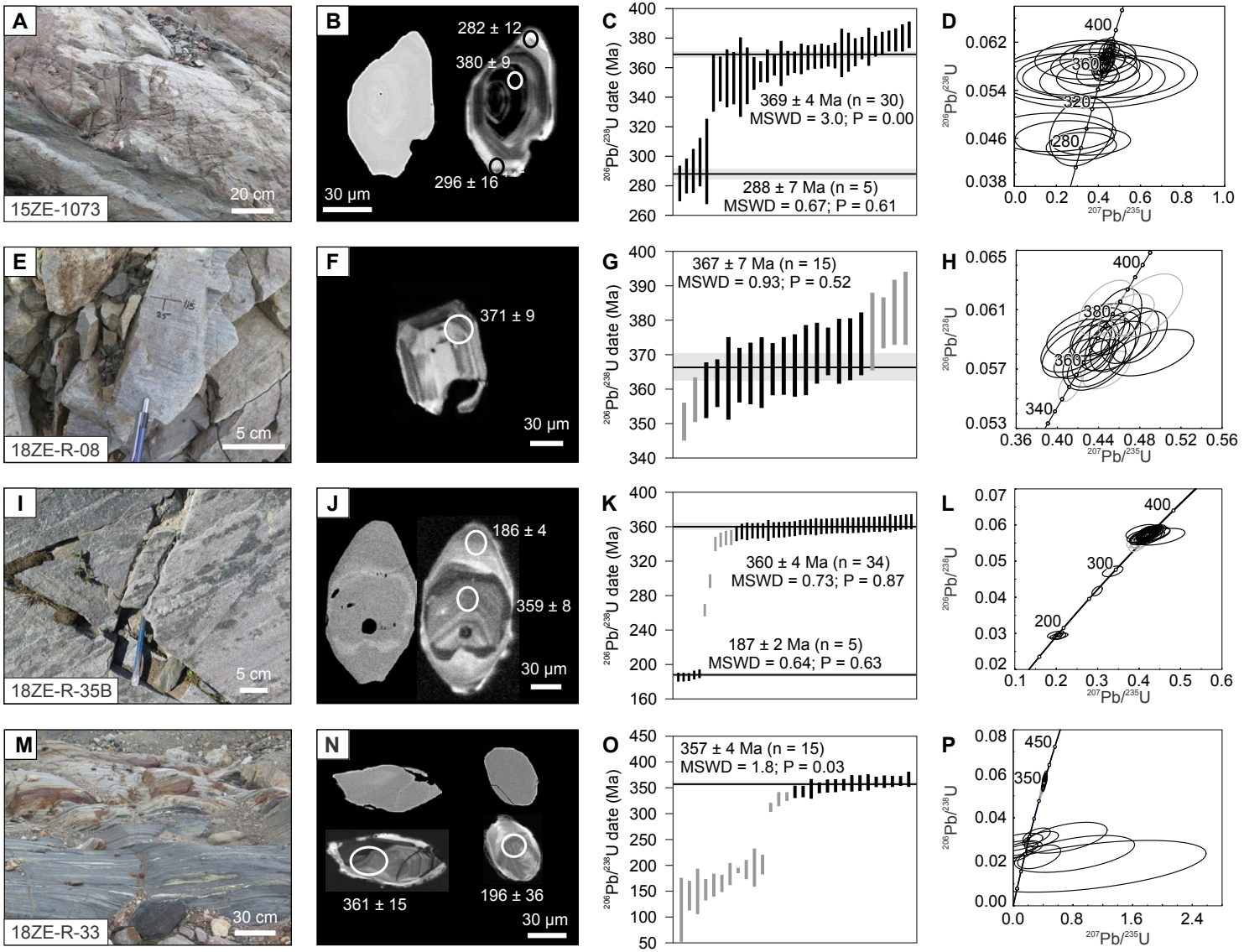

Figure 4. Meta-igneous rocks analyzed for U-Pb zircon geochronology. (A, E, I, M) Field photographs of sampled units. In A, note the foliation-parallel contact between the felsic orthogneiss (top right) and the amphibolite (bottom left). (B, F, J, N) Backscattered-electron (left or top, except for 18ZE-R-08) and cathodoluminescence (right or bottom) images of zircon with dates in Ma. Note metamorphic overgrowths on zircon from samples 15ZE-1073 and 18ZE-R-35B, and neograins of metamorphic zircon in sample 18ZE-R-33. (C, G, K, O) Weighted averages of $^{206}Pb/^{238}U$ dates. Older dates are interpreted as igneous crystallization ages; younger dates are interpreted as metamorphic ages. The uncertainties on the weighted mean date (gray band) and on individual dates are displayed at 2σ. MSWD—mean squared weighted deviation; *P*—probability of fit; *n*—number of analyses in the weighted average. (D, H, L, P) Concordia diagrams. Error ellipses are 2σ. Gray ellipses were not included in age calculations.

(Th/U = 0.57). The youngest zircon population consists of rare homogeneous to irregularly concentrically zoned overgrowths on older cores. Analyses on these overgrowths yielded dates ranging from 190 ± 4 Ma to 186 ± 4 Ma. The Th/U of the overgrowths ranged from 0.02 to 0.06 with an average of 0.04.

We interpret the Late Devonian to Mississippian population to be magmatic based on its euhedral morphology, oscillatory zoning, and high Th/U typical of magmatic zircon (Rubatto and Gebauer, 2000; Corfu et al., 2003; Hoskin and Schaltegger, 2003; Rubatto, 2017). In this population (weighted average date: 358 ± 4 Ma; MSWD = 2.1; P = 0.000; n = 38), four analyses are statistically younger and were likely affected by minor Pb loss. Excluding them gives an equivalent weighted average date of 360 ± 4 Ma without excess scatter (MSWD = 0.73; P = 0.87; n = 34; e.g., Wendt and Carl, 1991; Ludwig, 2003b), which we interpret to be most representative of the crystallization age of this sample (Figs. 4K and 4L).

The two Permian zircon dates do not overlap within error. Inspection of CL images, BSE images, and geochemical composition data suggests that these dates are not the result of mixed analyses of Late Devonian to Early Mississippian and Early Jurassic zircon. There is evidence for Permian metamorphism in the Florence Range suite (270–240 Ma; Soucy La Roche et al., 2022a) that could have promoted zircon (re)-crystallization of the grain dated at 264 ± 6 Ma; however, there is no known metamorphic event in that suite that overlaps the 297 ± 8 Ma date. Metamorphism at 288 ± 7 Ma is, however, recorded in the adjacent Boundary Ranges suite (sample 15ZE-1073 in this study).

The Early Jurassic population (weighted average date: 187 ± 2 Ma; MSWD = 0.64; P = 0.63; n = 5; Figs. 4K and 4L) has characteristics of metamorphic zircon (irregular zoning or absence of zoning, Th/U <0.06; Rubatto and Gebauer, 2000; Corfu et al., 2003; Hoskin and Schaltegger, 2003; Rubatto, 2017). This age likely represents metamorphic recrystallization associated with an Early Jurassic metamorphic event that is well documented by monazite, xenotime (Soucy La Roche et al., 2022a), and garnet (Dyer, 2020) ages in the area.

Sample 18ZE-R-33

Sample 18ZE-R-33 was collected from a well-foliated, 6-m-thick, medium-grained, hornblende-Bt-Pl-titanite-Qz (Hbl-Bt-Pl-Ttn-Qz) amphibolite layer within the Florence Range suite near Willison Glacier (Figs. 2 and 4M). Contacts with adjacent biotite gneiss and marble are parallel to the foliation.

Zircon forms two distinct populations (Fig. 4N). Zircon in the dominant population is 50–150 µm long and equant to elongate (1:1–3:1) and characterized by an oscillatory and patchy zoned core commonly overgrown by a thin (<10 µm) CL-bright homogeneous rim. The cores yielded dates ranging from 367 ± 14 Ma to 312 ± 8 Ma, with Th/U between 0.36 and 0.65 (average of 0.48), whereas the rims were too thin to be analyzed. No older xenocrystic cores were identified. We interpret the Carboniferous zircon population to be magmatic and the dates to represent the crystallization age of the amphibolite protolith based on their zoning pattern and Th/U >0.1 (Rubatto and Gebauer, 2000; Corfu et al., 2003; Hoskin and Schaltegger, 2003; Rubatto, 2017). The high MSWD and null P of the weighted average date (349 ± 8 Ma; MSWD = 9.5; P = 0.00; n = 18) indicate that there is excess scatter that cannot be attributed to analytical uncertainties (e.g., Wendt and Carl, 1991; Ludwig, 2003b). The three younger dates have high U (1500–2000 ppm) compared to older dates (300–1200 ppm) and compared to the calibration standard (<400 ppm). Excluding these three dates resulted in a statistically more reasonable weighted average date of 357 ± 4 Ma (MSWD = 1.8; P = 0.03; n = 15; Figs. 4O and 4P). We interpret this weighted average date as the best estimate of the crystallization age of the amphibolite protolith, though we acknowledge that there is still scatter beyond that attributed to analytical uncertainties (e.g., Wendt and Carl, 1991; Ludwig, 2003b).

A younger population is composed of 50–75 µm equant grains characterized by patchy or irregular oscillatory zoning and low Th/U (0.01–0.05; average 0.02). These analyses yielded imprecise dates ranging from 202 ± 18 Ma to 115 ± 60 Ma (n = 11; Figs. 4O and 4P). We interpret this population as metamorphic zircon, but because of the low precision of most dates, we do not assign it a definitive age. Early Jurassic metamorphic zircon crystallization is consistent with upper-amphibolite-facies metamorphism at ca. 190 Ma documented in the area (Soucy La Roche et al., 2022a; Dyer, 2020).

GEOCHEMISTRY

Amphibolite-facies metamorphism and deformation in the Florence Range, Boundary Ranges, and Whitewater suites (Currie, 1994; Mihalynuk et al., 1999; Dyer, 2020; Soucy La Roche et al., 2022a) preclude the identification of specific protoliths using field observations and petrography. Geochemistry, on the other hand, can be used to differentiate protoliths of the different metamorphic suites and provide insights into the tectonic setting of their formation. Metamorphism may have resulted in element mobility; therefore, immobile trace elements are preferred for interpretations (Th, Nb, La, Ce, Nd, Sm, Zr, Hf, Eu, Ti, Gd, Dy, Y, Er, Yb, Lu, V, and Sc; e.g., Pearce, 1996, 2014).

Analytical Methods

Fist-sized sample fragments with weathered surfaces removed and free of visible alteration were used to characterize the bulk-rock chemical composition. Samples from the Florence and Boundary Ranges suites (sample numbers starting with 18ZE-R-) were analyzed by Activation Laboratories, Ltd. (Ancaster, Ontario, Canada) in 2018. These samples were crushed, split, pulverized with mild steel, and fused using lithium metaborate/tetraborate fusion in Pt crucibles. The resulting molten bead was digested in a weak nitric acid solution. Major oxides were measured with ICP–optical emission spectrometry (OES) on a Thermo Jarrell-Ash ENVIRO II ICP or a Varian Vista 735 ICP, and trace elements were measured by ICP-MS on a Perkin Elmer Sciex ELAN 6000,

6100, or 9000 ICP-MS. The major elements of metapelitic samples reported herein were analyzed by wavelength-dispersive X-ray fluorescence (XRF) on a Panalytical Axios Advanced XRF. Results of replicate analyses and reference materials run as unknowns are available in Table S3.

Samples from the Whitewater suite (sample numbers starting with ZE10-R) and additional samples from the Boundary Ranges suite (sample numbers starting with ZE10- and 15ZE-) were analyzed by ICP-OES and ICP-MS following lithium metaborate/tetraborate fusion at Acme (Bureau Veritas, Vancouver, British Columbia, Canada) in 2010 and Activation Laboratories, Ltd., in 2011 and 2016, respectively. Complete analytical details and certificates of analysis are available in Zagorevski (2016, 2018).

Sample Description

Samples were divided into three main groups for geochemical characterization (Table S3). The first group is characterized by abundant mafic minerals (e.g., chlorite, hornblende, and pyroxene, depending on metamorphic grade) and generally low (<55%) SiO_2. As such, we call this group "amphibolite," although some samples contain continuous quartz-rich layers and have SiO_2 >55%, which indicate these samples may not be pure meta-mafic rocks. Amphibolite from the Florence Range suite is generally medium to coarse grained (matrix grain size 500–5000 µm) and well foliated, with common porphyroblasts of garnet in a matrix of hornblende, plagioclase, biotite, and opaques ± clinopyroxene, ± quartz, ± titanite (Fig. 4M). One sample was dated at 357 ± 4 Ma (18ZE-R-33; this study). Amphibolite from the Boundary Ranges suite is generally fine grained (matrix grain size <1000 µm) and well foliated, with common porphyroblasts of hornblende and garnet in a matrix of hornblende, plagioclase, epidote, and opaques ± chlorite, ± biotite, ± quartz (Fig. 5A). Amphibolite from the Whitewater suite is medium-grained (matrix grain size 100–3000 µm) and weakly foliated, with common millimeter- to centimeter-scale porphyroblasts of garnet, hornblende, plagioclase, and epidote in a matrix of the same finer-grained minerals in addition to rare quartz and titanite (Fig. 5B). Where present, chlorite was replaced by hornblende and epidote, or it replaced garnet, epidote, and hornblende.

The second group comprises felsic to intermediate orthogneiss from the Florence and Boundary Ranges suites. Contacts between orthogneiss and adjacent units, where exposed, are commonly parallel to the foliation, impeding the assessment of their structural relationships. However, the orthogneiss contains millimeter- to centimeter-scale feldspar porphyroclasts (Fig. 5C) and, in the Boundary Ranges suite, decimeter-scale xenoliths of the host chlorite schist, consistent with a metaplutonic origin (Fig. 5D). One of the two samples from the Florence Range suite (18ZE-R-35B) was dated at 360 ± 4 Ma (this study) and described in a previous section. The other sample (18ZE-R-35A) was collected in an adjacent layer and is similar except for the presence of centimeter-sized K-feldspar porphyroclasts (Fig. 5C). Boundary Ranges suite gneiss is more leucocratic and includes the 367 ± 7 Ma sample 18ZE-R-08 and 369 ± 4 Ma sample 15ZE-1073 (this study). Similar orthogneiss samples from that area yielded variably discordant Late Devonian to Early Mississippian U-Pb zircon dates interpreted as igneous crystallization ages (Currie and Parrish, 1997).

The third group includes metapelite, metapsammite, and quartzite from the Florence Range, Boundary Ranges, and Whitewater suites collectively referred to as metasedimentary units. Metapelite and metapsammite in the Florence Range suite are coarse-grained, mica-rich, migmatitic gneisses with a well-developed foliation (Fig. 5E). Mineral assemblages contain a wide variety of metamorphic minerals such as biotite, white mica, plagioclase, quartz, garnet, kyanite, sillimanite, andalusite, cordierite, staurolite, K-feldspar, and graphite. Several representative samples were described in detail by Soucy La Roche et al. (2022a) and Dyer (2020). Metapelite and metapsammite in the Boundary Ranges suite are characterized by a lower metamorphic grade and finer grain size (Fig. 5F). Metamorphic mineral assemblages commonly contain biotite, white mica, plagioclase, quartz, garnet, epidote, graphite, and rarely andalusite (Dyer, 2020). Metapelite from the Whitewater suite is fine-grained, interlayered with quartzite, and it contains quartz, muscovite, plagioclase, sulfides, graphite, garnet, biotite, epidote, and chlorite. Quartzite is only present in the Florence Range and Whitewater suites. All quartzite samples are dominated by quartz, and they contain variable amounts of muscovite, biotite, garnet, and epidote. In addition, quartzite from the Florence Range suite (Fig. 5G) contains plagioclase, whereas quartzite from the Whitewater suite contains chlorite and Mn-rich epidote (piemontite) (Fig. 5H). One sample from the Florence Range suite contains distinctive graphite layers (Fig. 5I).

Geochemical data were also acquired from additional Hbl-Pl-Qz gneiss samples in the Florence Range suite within the Wann River shear zone, but it is not clear if these units are Late Devonian to Early Mississippian orthogneiss, Permian Wann River gneiss, or Early Jurassic Tagish Lake suite. For example, the area where sample 18ZE-R-35B was collected was originally mapped as Florence Range suite (Currie, 1994) and reinterpreted as Permian Wann River gneiss (Mihalynuk et al., 1999; Cui et al., 2017), but this sample was dated at 360 ± 4 Ma (this study), consistent with Florence Range suite. In the absence of timing constraints, geochemical data from these samples are reported in Table S3, but they were not used for interpretations.

Results

Amphibolite

Extended trace-element profiles of amphibolite samples were normalized to N-MORB (Sun and McDonough, 1989) with the addition of V and Sc concentrations based on Klein (2004). This normalization factor is the most intuitive, best highlights variations between key elements, and is overall the most useful to compare suites of samples and infer their tectonic setting (e.g., Pearce, 2008, 2014; Zagorevski and van Staal, 2021).

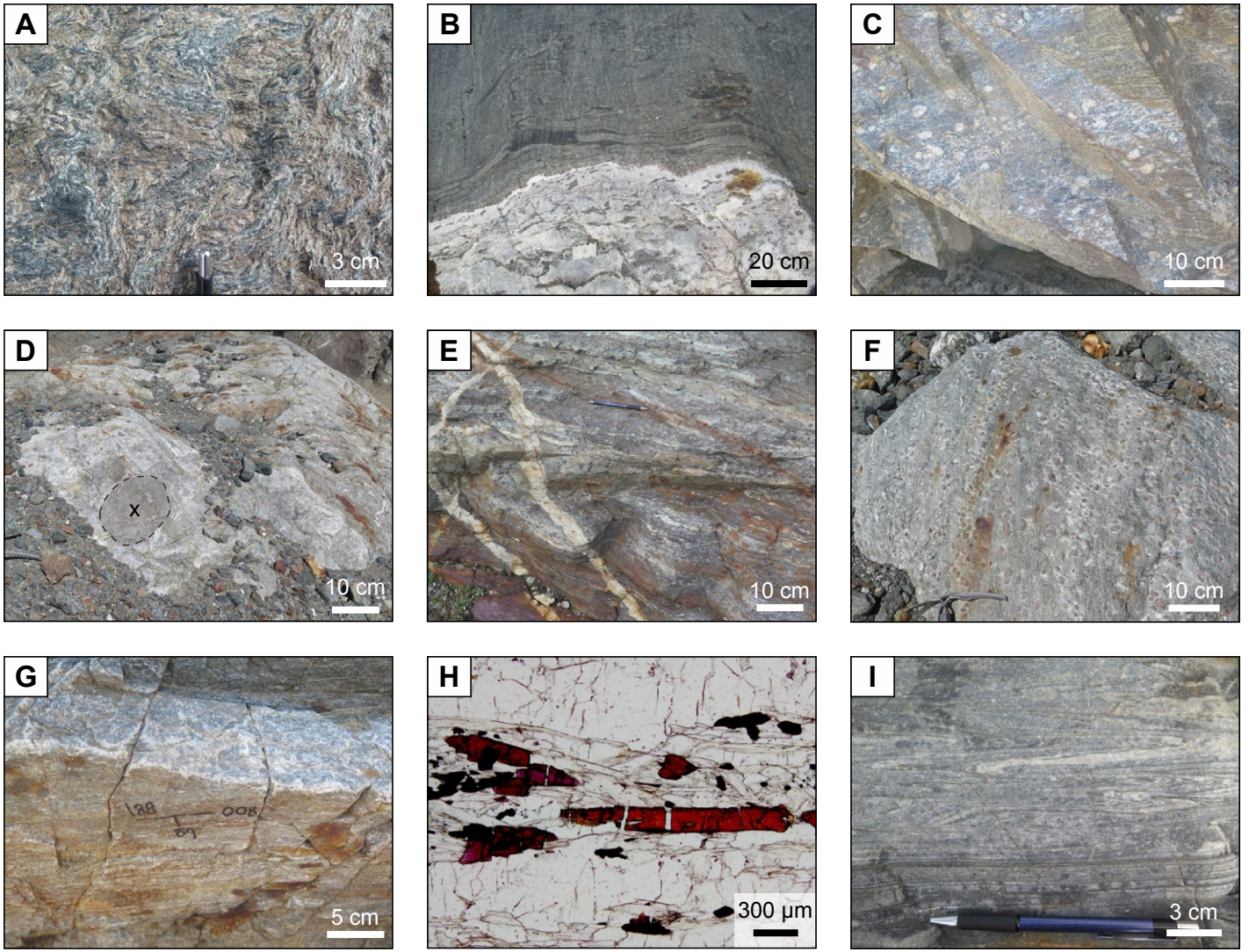

Figure 5. Representative field photographs and photomicrographs of units from all three suites. (A) Boundary Ranges suite amphibolite. (B) Whitewater suite amphibolite (top) and quartzite (bottom). (C) Florence Range suite mesocratic orthogneiss from which sample 18ZE-R-35A was collected. This orthogneiss is similar to sample 18ZE-R-35B used for geochronology, except that it contains porphyroclasts of K-feldspar. (D) Boundary Ranges suite orthogneiss containing a round xenolith (X) of the host schist, outlined with a dashed line. (E) Florence Range suite garnet-biotite gneiss (metapelite) crosscut by Cretaceous to Eocene (?) felsic dikes. (F) Boundary Ranges suite garnet-muscovite-chlorite schist (metapelite). (G) Florence Range suite quartzite interpreted as meta-arenite. (H) Piemontite in Whitewater suite quartzite interpreted as meta-chert. (I) Florence Range suite graphitic quartzite interpreted as meta-chert. Note isoclinal folds.

Florence Range suite amphibolite samples were separated in two types. Type 1 amphibolite (n = 6; 18ZE-R-25A, 18ZE-R-25C, 18ZE-R-33, 18ZE-R-44, 18ZE-R-49C, 18ZE-R-64) is characterized by enriched Th and light rare earth elements (LREEs) relative to heavy REEs (HREEs), absence of Nb, Eu, Zr, or Hf anomalies, and a positive V anomaly (Fig. 6A). One sample (18ZE-R-49C) classified as type 1 amphibolite has a steeper LREE to middle REE (MREE) negative slope, and a flat to slightly positive MREE to HREE slope, but it also displays the most striking features of type 1 amphibolite, such as the absence of a Nb anomaly. Type 2 amphibolite (n = 2; 18ZE-R-28, 18ZE-R-34) is characterized by enriched Th and LREEs relative to HREEs, negative Nb and Ti anomalies, slightly positive Zr and Hf anomalies, and the absence of a V anomaly (Fig. 6A). On the Zr/Ti versus Nb/Y discrimination diagram for rock types of Pearce (1996), type 1 amphibolite plots in the alkaline basalt field, except one sample that plots in the basalt field (Fig. 6B). Type 2 amphibolite plots in the basalt and andesite + basaltic andesite fields. On the La-Y-Nb discrimination diagram for tectonic settings of basalts (Cabanis and Lecolle, 1989), type 1 amphibolite plots in the alkaline intercontinental rifts and continental fields, whereas type 2 amphibolite plots in the calc-alkaline field (Fig. 6C). On the Th/Yb versus Nb/Yb discrimination diagram of Pearce (2008, 2014), type 1 amphibolite plots in the mantle array close to the OIB composition, and type 2 amphibolite plots in the continental arc field (Fig. 6D).

Boundary Ranges suite amphibolite samples were separated in two types. Type 1 amphibolite (n = 5; 18ZE-R-09, 18ZE-R-59, 18ZE-R-60, 18ZE-R-85A,18ZE-R-85C) is characterized by weakly enriched Th and LREEs relative to HREEs, a strongly negative Nb anomaly, weakly negative Zr, Hf, and Ti anomalies, absence of or weakly positive Eu anomaly, and strongly positive V and Sc anomalies (Fig. 6E). Type 2 amphibolite (n = 7; 18ZE-R-11B, 18ZE-R-19, 18ZE-R-20, 18ZE-R-85D, ZE10–229B, 15ZE-1075, 15ZE-1077) is characterized by enriched Th and LREEs relative to HREEs, negative Nb, Zr, Hf, and Ti anomalies, and slightly positive Eu anomaly, though the positive Eu anomaly looks exaggerated because of the adjacent strongly negative Zr, Hf, and Ti anomalies (Fig. 6E). Most type 2 amphibolite samples have positive V and Sc anomalies, but two samples exhibit the opposite. On the Zr/Ti versus Nb/Y discrimination diagram for rock types of Pearce (1996), both types of amphibolite plot in the basalt field, except one type 2 amphibolite sample, which plots in the basalt and andesite + basaltic andesite field (Fig. 6B). On the La-Y-Nb discrimination diagram for tectonic settings of basalts (Cabanis and Lecolle, 1989), type 1 amphibolite straddles the IAT and IAT-to-calc-alkaline transitional fields, whereas type 2 amphibolite plots in the

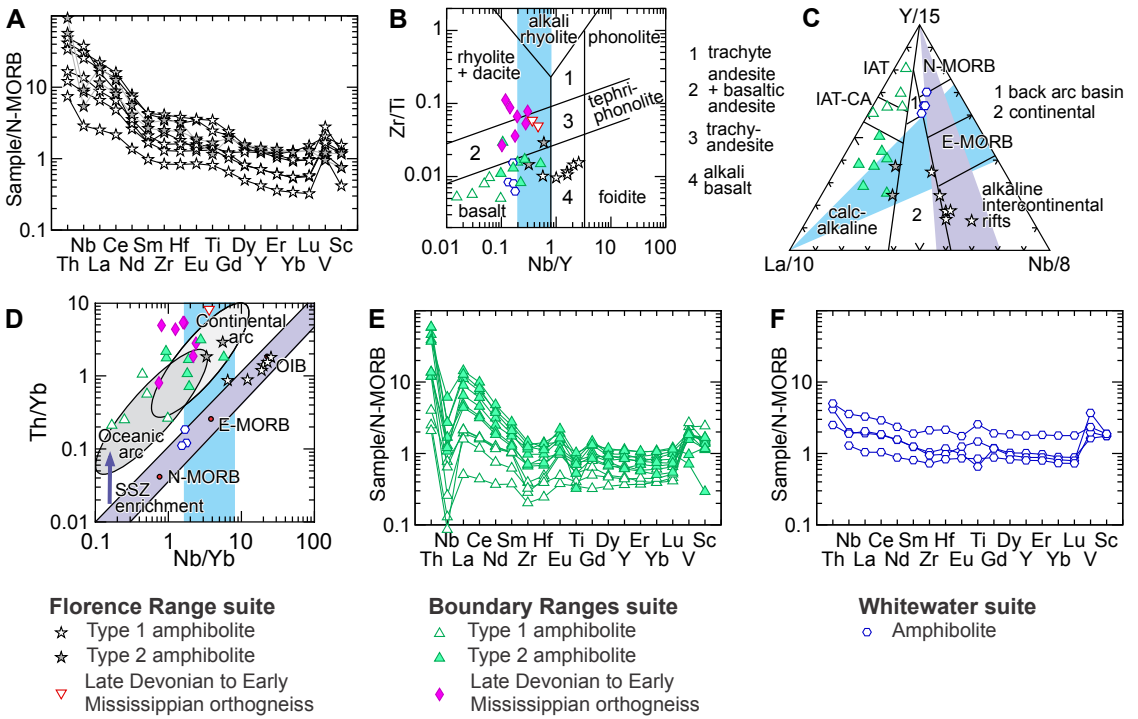

Figure 6. Geochemical composition of amphibolite. (A, E, F) Extended trace-element profiles of amphibolite samples from the Florence Range suite (A), Boundary Ranges suite (E), and Whitewater suite (F) normalized to normal mid-ocean-ridge basalt (N-MORB; Sun and McDonough, 1989) with the addition of V and Sc concentrations based on Klein (2004). (B) Zr/Ti vs. Nb/Y discrimination diagram for rock types (Pearce 1996). (C) La-Y-Nb discrimination diagram for tectonic settings of basalt (Cabanis and Lecolle, 1989). (D) Th/Yb vs. Nb/Yb discrimination diagram (Pearce, 2008, 2014). Blue fields in B–D represent equivalent Nb/Y ratio, a proxy for alkalinity increasing toward higher Nb/Y ratio. Purple fields in C–D represent mantle array equivalence. CA—calc-alkaline; E-MORB—enriched mid-ocean-ridge basalt; IAT—island-arc tholeiite; N-MORB—normal mid-ocean-ridge basalt; OIB—oceanic-island basalt; SSZ—suprasubduction zone.

calc-alkaline field (Fig. 6C). On the Th/Yb versus Nb/Yb discrimination diagram of Pearce (2008, 2014), both types of amphibolite plot above the mantle array and trend from the oceanic arc (type 1) to continental arc (type 2) fields (Fig. 6D).

Whitewater suite amphibolite (n = 4; ZE10-R011, ZE10-R017A, ZE10-R018, ZE10-R022) is characterized by extended trace-element profiles similar to that of N-MORB, except for a slight enrichment in Th, Nb, and LREEs relative to HREEs (Fig. 6F). Only one sample shows a faint negative Nb anomaly. Ti is slightly variable and exhibits weakly positive, negative, or no anomaly. A positive V anomaly is also characteristic of this suite. These amphibolite samples plot in the basalt field of the Zr/Ti versus Nb/Y discrimination diagram for rock types of Pearce (1996) (Fig. 6B). On the La-Y-Nb discrimination diagram for tectonic settings of basalts (Cabanis and Lecolle, 1989), they plot at the intersections of the E-MORB, N-MORB, and back-arc basin basalt (BABB) fields (Fig. 6C). On the Th/Yb versus Nb/Yb discrimination diagram of Pearce (2008, 2014), Whitewater suite amphibolite plots in the mantle array halfway between the N-MORB and E-MORB compositions (Fig. 6D).

Felsic to Intermediate Orthogneiss

On a N-MORB–normalized diagram, felsic to intermediate orthogneiss (Florence Range suite: n = 2, 18ZE-R-35A, 18ZE-R-35B; Boundary Ranges suite: n = 7, 18ZE-R-06, 18ZE-R-08, 18ZE-R-10, 18ZE-R-15, 18ZE-R-23, ZE10–229A, ZE10–230) is characterized by enriched Th and LREEs relative to HREEs, strongly negative Nb and Ti anomalies, absent to slightly positive Zr and Hf anomalies, and negative V and Sc anomalies (Fig. 7A). Florence Range suite samples are more enriched in LREE and have negative HREE slopes, whereas Boundary Ranges suite samples exhibit slightly positive HREE slopes. On an extended trace-element diagram normalized to the average upper continental crust (UCC; Taylor and McLennan, 1985; McLennan, 2001), Florence Range suite samples show a negative LREE to HREE slope, whereas samples from the Boundary Ranges suite show a positive slope (Fig. 7B). Samples plot in the basalt, andesite + basaltic andesite, and rhyolite + dacite fields on the Zr/Ti versus Nb/Y discrimination diagram for rock types of Pearce (1996) (Fig. 6B). On the Th/Yb versus Nb/Yb discrimination diagram of Pearce (2008, 2014), Boundary Ranges suite orthogneiss plots above the mantle array at the intersection of the oceanic and continental arc fields or above it (Fig. 6D). Both samples from the Florence Range suite plot above the continental arc field (sample 18ZE-R-35B plots outside the range of the plot due to Th/Yb = 22.5). On the Ta versus Yb discrimination of Pearce et al. (1984), orthogneiss samples from both suites plot in the volcanic arc granite field (Fig. 7C).

Metasedimentary Rocks

Metasedimentary rocks include metapelites and metapsammites from the Florence Range (n = 21), Boundary Ranges (n = 14), and Whitewater (n = 3)

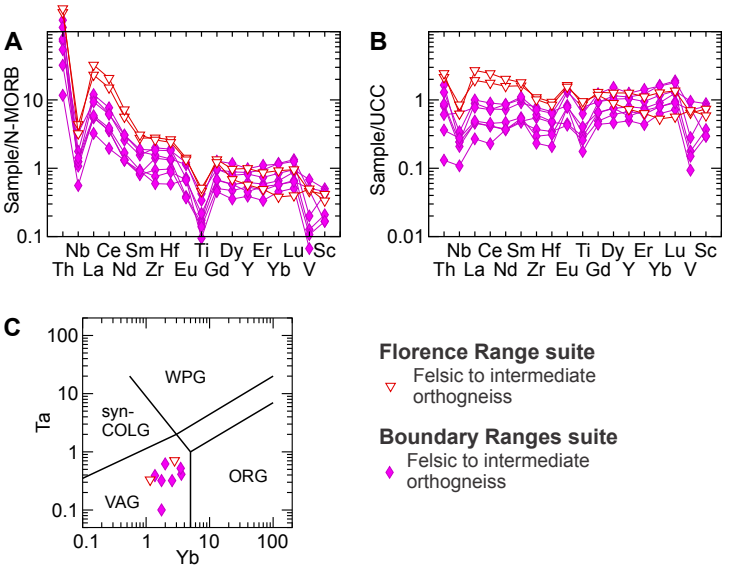

Figure 7. Geochemical composition of felsic to intermediate orthogneiss. (A) Extended trace-element profiles of orthogneiss samples from the Florence Range and Boundary Ranges suites normalized to normal mid-ocean-ridge basalt (N-MORB; Sun and McDonough, 1989) with the addition of V and Sc concentrations based on Klein (2004). (B) Extended trace-element profiles of orthogneiss samples from the Florence Range and Boundary Ranges suites normalized to upper continental crust (UCC; Taylor and McLennan, 1985; McLennan, 2001). (C) Ta vs. Yb discrimination for tectonic settings of granite (Pearce et al., 1984). VAG—volcanic arc granite; syn-COLG—syncollision granite; WPG—within-plate granite; ORG—ocean ridge granite.

suites and quartzite from the Florence Range (n = 6) and Whitewater (n = 5) suites. Extended trace-element diagrams normalized to N-MORB and UCC (Taylor and McLennan, 1985) are provided in Figure S3. On the sedimentary rock classification diagram of Herron (1988), metapelite and metapsammite samples from the Florence Range and Whitewater suites plot mainly in the shale and wacke fields, whereas samples from the Boundary Ranges suite plot in the shale and Fe-shale fields (Fig. 8A). Quartzite samples from the Florence Range suite plot within or close to the sublitharenite field, and those from the Whitewater suite plot in the sublitharenite, Fe-sandstone, and quartz arenite fields (Fig. 8A). On a Th/Sc versus La/Sc diagram (e.g., Piercey and Colpron, 2009), metapelite, metapsammite, and quartzite samples from the Florence Range and Whitewater suites coincide with the average composition of UCC and post-Archean Australian shale (PAAS; Taylor and McLennan, 1985) or plot slightly above and below them, respectively (Fig. 8B). Boundary Ranges suite samples are more dispersed and form an array from the composition of UCC and PAAS toward the composition of Boundary Ranges suite amphibolite

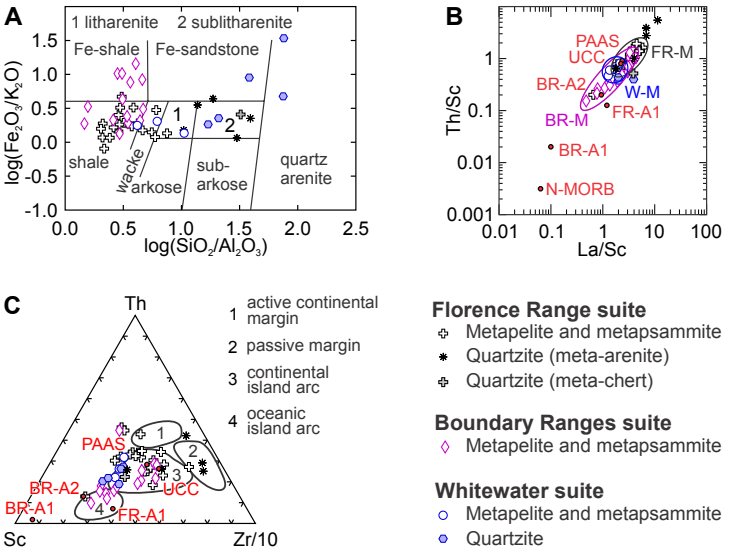

Figure 8. Geochemical composition of metasedimentary rocks. (A) Sedimentary rock classification diagram (Herron, 1988). (B) Th/Sc vs. La/Sc diagram (Piercey and Colpron, 2009). (C) Th-Sc-Zr ternary discrimination diagram for tectonic settings of graywackes (Bhatia and Crook, 1986). In B and C, values for average composition of upper continental crust (UCC; Taylor and McLennan, 1985), post-Archean Australian shale (PAAS; Taylor and McLennan, 1995), type 1 amphibolite from the Florence Range suite (FR-A1), and types 1 and 2 amphibolite from the Boundary Ranges suite (BR-A1 and BR-A2, respectively) are shown for reference. N-MORB—normal mid-ocean-ridge basalt.

(Fig. 8B). The relative enrichment of Sc in Boundary Ranges and Whitewater suites samples compared to Florence Range suite samples is also illustrated on a Th-Sc-Zr ternary diagram (Fig. 8C; Bhatia and Crook, 1986). In addition, the Th-Sc-Zr ternary diagram highlights the Zr enrichment in Florence Range suite quartzite samples compared to all other metasedimentary samples (Fig. 8C).

Interpretation

Amphibolite

Most amphibolite samples from this study plot in the basalt and alkaline basalt fields, with few exceptions that plot in the andesite + basaltic andesite field (Fig. 6B). Mafic igneous rocks are most directly linked genetically to the underlying mantle and are the most reliable indicators of tectonic settings. Immobile trace elements and their ratios can be used as fingerprints of magmatic and tectonic processes (Cann, 1970; Pearce, 1996). Mafic discrimination diagrams utilize volcanic rocks or rocks with liquid-like compositions (Pearce, 1996), which can be difficult to identify in highly metamorphosed areas. We relied on chemical indicators of cumulate compositions as outlined in Pearce (1996) to identify nonvolcanic protoliths.

Amphibolite in the Florence Range, Boundary Ranges, and Whitewater suites is characterized by distinct geochemical compositions. The enrichment of LREEs, high Nb/La, and absence of a Nb anomaly in type 1 amphibolite from the Florence Range suite are consistent with an OIB chemical composition (Fig. 6A). Considering that Florence Range type 1 amphibolite is associated with continentally derived siliciclastic rocks, the Florence Range suite type 1 amphibolite likely formed in a continental rift setting (Figs. 6A, 6C, and 6D), away from a subduction zone. The steeper LREE-MREE negative slope and flat MREE-HREE slope of sample 18ZE-R-49C compared to other type 1 amphibolite samples may be explained by a higher proportion of garnet melting at the source because garnet is a major HREE sink in the mantle (e.g., Pearce, 1996). Type 2 amphibolite is characterized by a weakly negative Nb anomaly (Fig. 6A). Although a negative Nb anomaly is typical of arc volcanism (Pearce, 1996), these rocks are anomalously rich in Th and LREEs compared to volcanic arc rocks (Th up to 100× the value of N-MORB). The weakly negative Nb anomaly could be explained by fractionation of Ti-rich phases such as titanite, rutile, or ilmenite (Green and Pearson, 1987). Alternatively, the weak Nb anomaly may be the result of crustal contamination of magma with an OIB composition (i.e., type 1 amphibolite). Amphibolite with an OIB composition variably contaminated by crustal material is common in the Yukon Territory part of the Yukon-Tanana terrane (e.g., Piercey et al., 2002, 2004) and in the Yukon-Tanana Upland of Alaska (e.g., Dusel-Bacon and Cooper, 2000, 2004). Altogether, these geochemical data suggest that amphibolite in the Florence Range suite formed in a continental rift setting.

Type 1 amphibolite from the Boundary Ranges suite has negative Zr, Hf, and Ti anomalies, which points to fractionation of the parental magma, and a positive Sc anomaly, which suggests an enrichment in clinopyroxene (Fig. 6E; Pearce, 1996). These anomalies suggest that type 1 amphibolite may be metamorphosed gabbro rather than basalt, and discrimination diagrams should be used with caution. Overall, the enrichment of Th and La relative to Nb in type 1 amphibolite samples from the Boundary Ranges suite suggests an oceanic volcanic arc setting (Figs. 6C–6E). However, these compositions are not restricted to active volcanic arc rocks because a metasomatized mantle signature can be inherited from previous subduction events. For example, a compilation of geochemical data from well-constrained modern tectonic settings demonstrates that basalts erupted in continental rift settings can plot in the fields typical of volcanic arc basalt (Zagorevski and van Staal, 2021). Type 2 amphibolite differs from type 1 based on its more evolved (i.e., more enriched in Th and LREEs) and more alkaline (i.e., less enriched in Nb relative to Y and Yb) composition (Fig. 6E). The chemical composition of type 2 amphibolite could be the result of mixing between type 1 amphibolite and metasedimentary material of the Boundary Ranges suite (Fig. 9). This mixing is consistent with the generally higher SiO_2, Al_2O_3, quartz, and mica contents of type 2 amphibolite compared to type 1 amphibolite (Table S3).

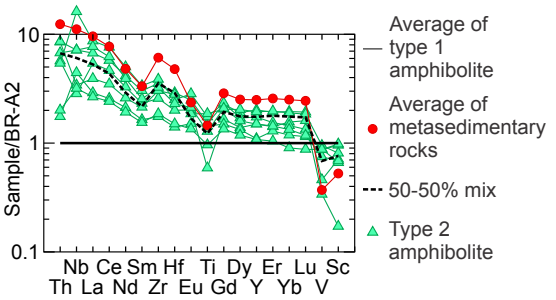

Figure 9. Extended trace-element profiles of a modeled 50%–50% mix of the average composition of metasedimentary rocks from the Boundary Ranges suite with the average composition of type 1 amphibolite from the same suite (BR-A2, normalization factor). Type 2 amphibolite has a similar chemical composition to that mix.

The Whitewater suite amphibolite samples plot in the tectonic fields of MORB and BABB in discrimination diagrams (Fig. 6C). The slight enrichment in Th and LREEs and the weakly negative Nb anomaly in some samples (Fig. 6F) could be the result of melting of MORB mantle with a variable subduction component or mixing of MORB mantle and subduction-modified mantle sources, two processes common in back-arc basin settings (Pearce, 1996).

Felsic to Intermediate Orthogneiss

The chemical composition of felsic to intermediate rocks is controlled by the tectonic setting and several other competing processes, including continental crust contamination, mixing of melt sources from different continental lithological units, and accessory mineral fractionation and removal from the melt (Pearce et al., 1984). Most chemical anomalies can be produced by several processes, and, as such, identifying the tectonic setting in which felsic to intermediate magmas formed is much less straightforward than with mafic magmas. The chemical composition of orthogneiss samples from the Florence Range and Boundary Ranges suites is characterized by enriched Th and LREEs and a negative Nb anomaly (Figs. 7A and 7B), indicative of an enriched mantle source, contamination by continental crust, or fractionation of Ti-rich minerals. This composition is compatible with multiple tectonic settings, including a continental volcanic arc or a continental rift (e.g., Hawkesworth et al., 1995; Hooper et al., 1995). The two suites have distinct extended trace-element profiles, best illustrated on a UCC-normalized diagram, on which the Florence Range suite samples have a negative LREE-HREE slope and the Boundary Ranges sample have a positive LREE-HREE slope (Fig. 7B). It is therefore doubtful that the Florence Range suite samples represent a more evolved component of a common magmatic suite.

Metasedimentary Rocks

The composition of metasedimentary rocks reflects the source of the sediments and can be used to assess the contributions of upper-crustal sources that are enriched in incompatible elements such as Th, Zr, and La versus mafic sources that are enriched in Sc (e.g., Piercey and Colpron, 2009, and references therein). Metapelite and metapsammite from the Florence Range suite have a chemical composition similar to UCC and PAAS (Figs. 8B and 8C; Fig. S3), indicating that the protolith source was dominated by continental crust. In contrast, the relative enrichment in Sc of Boundary Ranges suite samples compared to UCC and PAAS (Figs. 8B and 8C) indicates a contribution from a mafic source. Their range of compositions overlaps the composition of Boundary Ranges suite type 2 amphibolite and trends toward the composition of type 1 amphibolite, consistent with a depositional environment close to a volcanic source similar to the Boundary Ranges suite amphibolite. Metapelite in the Whitewater suite has a composition weakly enriched in Sc compared to UCC and PAAS (Figs. 8B and 8C), consistent with an upper continental crust source potentially mixed with a small component of a mafic source.

Most quartzite samples from the Florence Range suite are depleted in Sc and enriched in La, Th, and Zr compared to other metasedimentary rocks (Figs. 8B and 8C), consistent with a higher proportion of heavy minerals in quartz-rich sediments (Bhatia and Crook, 1986), and they are as such interpreted as meta-arenite. One petrographically distinct quartzite sample from the Florence Range suite has higher La relative to Th, higher Sc (Figs. 8B and 8C), and a different extended trace-element profile (Fig. S3). It contains abundant graphite but no plagioclase, and it is most likely a meta-chert. In contrast to the Florence Range suite, Whitewater suite quartzite is depleted in Th, La, and Zr relative to the average UCC and PAAS (Figs. 8B and 8C). The presence of piemontite (Fig. 5H), a common mineral in metamorphosed Mn-rich chert (Bonazzi and Menchetti, 2004), suggests that Whitewater suite quartzite is meta-chert.

DISCUSSION

Age and Origin of Protoliths

Pre- to Late Devonian

The Florence Range suite is predominantly composed of metasedimentary rocks with minor amphibolite and orthogneiss. The youngest detrital zircon dates (excluding metamorphic overgrowths) from quartzofeldspathic schist indicate a late Neoproterozoic or younger depositional age. The minimum depositional age is constrained by the age of orthogneiss (18ZE-R-35B), which we interpret to have intruded the Florence Range suite at 360 ± 4 Ma. This orthogneiss contained one discordant inherited zircon grain dated at 1735 ± 64 Ma that was either assimilated from the host Florence Range suite

or its unexposed basement. The provenance and chemical composition of the metasedimentary rocks indicate that they were derived from continental crust, either directly or through recycling of continentally derived sediment. The association of abundant pelite, psammite, quartz arenite, and carbonate points to a continental margin origin (e.g., Currie, 1994).

In the Boundary Ranges suite, felsic orthogneiss (367 ± 7 Ma and 369 ± 4 Ma) (e.g., Fig. 5D) constrains the minimum age of amphibolite and metasedimentary rocks to Late Devonian or older, but the maximum age is unconstrained. The chemical compositions of Boundary Ranges suite metasedimentary rocks indicate that they were in part derived from mafic rocks with a similar composition to the Boundary Ranges suite amphibolite. Although type 1 amphibolite in the Boundary Ranges suite has a likely plutonic origin, extrusive equivalents of these amphibolite units may have supplied the mafic component to the sedimentary units. Overall, pre–Late Devonian metasedimentary rocks of the Boundary Ranges suite were deposited in proximity to a mafic volcanic source, in strong contrast to the pre–Late Devonian metasedimentary rocks of the Florence Range suite.

The Whitewater suite formed in a third, distinct tectonic environment. The amphibolite composition is characteristic of BABB (Figs. 6C and 6F). Interlayering of BABB amphibolite, manganiferous meta-chert, and graphite-rich metapelite suggest deposition in a volcanically active, anoxic marine basin, such as a spreading center or near a guyot. The Whitewater suite lacks geochronological constraints but is presumed to be Paleozoic or older (Mihalynuk et al., 1994).

Overall, our data demonstrate that the pre–Late Devonian Florence Range, Boundary Ranges, and Whitewater suites formed in distinct tectonic settings. However, the ages of the protoliths are still poorly constrained; therefore, it is possible that these were not contemporaneous tectonic environments.

Late Devonian to Early Mississippian

The Late Devonian to Early Mississippian magmatism was characterized by calc-alkaline characteristics in both the Florence Range (360 ± 4 Ma) and Boundary Ranges (369 ± 4 Ma and 367 ± 7 Ma) suites (Figs. 6 and 7). The age of these orthogneiss protoliths do not overlap within error, based on the two higher-precision ages, and their extended trace-element profiles are different (Fig. 7B), suggesting that they were not part of the same magmatic suite, and that the Florence Range and Boundary Ranges suites may not have been together at that time. Calc-alkaline magmatism is compatible with continental arc or continental rift settings. OIB magmatism (357 ± 4 Ma; Figs. 6A, 6C, and 6F) is restricted to the Florence Range suite and is within error or a few million years younger than calc-alkaline magmatism, which may indicate two distinct tectonic possibilities. It is possible that the Florence Range suite calc-alkaline magmatism represents a continental arc that formed on Laurentia-derived sediments and subsequently rifted, leading to OIB magmatism of the passive margin of the back-arc rift. Such a model, based on the opening of the Sea of Japan (e.g., Pouclet et al., 1994), has been previously proposed for the Yukon-Tanana terrane in Yukon and NE British Columbia (e.g., Nelson, 1993; Piercey et al., 2004). Alternatively, the calc-alkaline arc-like characteristics of the Florence Range suite orthogneiss may have been inherited from melting of previously metasomatized mantle and/or continental crust (e.g., Hawkesworth et al., 1995; Hooper et al., 1995). In this scenario, OIB magmatism may represent upwelling of enriched mantle below a continental rift.

Overall, our data suggest that the Florence Range and Boundary Ranges suites were likely separate during the Late Devonian to Early Mississippian. The Florence Range suite was located in a continental rift setting away from a subduction zone. Although the Boundary Ranges suite may have been part of a continental arc at that time, our data cannot rule out inherited subduction zone signature in a continental rift. The lack of geochronological constraints on the Whitewater suite precludes the assessment of its relationship with the Florence Range and Boundary Ranges suites during the Late Devonian to Early Mississippian.

Unusual Detrital Zircon Signature of Florence Range Suite Quartzofeldspathic Schist and Correlation with the Snowcap Assemblage

Pre- to Late Devonian Florence Range suite continental margin metasedimentary units intruded by Late Devonian to Early Mississippian calc-alkaline and alkaline (OIB) magmatic units are correlative to the Snowcap assemblage of the Yukon-Tanana terrane (e.g., Dusel-Bacon et al., 2004, 2006; Nelson et al., 2006, 2013; Piercey et al., 2002, 2004; Piercey and Colpron, 2009). The detrital zircon population in the Florence Range suite is dominated by 1.5–1.0 Ga zircon, with secondary Neoarchean and late Paleoproterozoic peaks (Fig. 10A). Late Mesoproterozoic zircon probably originated ultimately from the Grenville orogen, on the SE margin of Laurentia, because it is the only orogenic belt of that age in Laurentia, and it was an incredibly fertile zircon source (Whitmeyer and Karlstrom, 2007; Dickenson, 2008; Rivers et al., 2012).

Detrital zircon data from the Florence Range suite are strikingly different from the Snowcap assemblage in Yukon (see compilations in LaMaskin, 2012; Cleven et al., 2019; Ryan et al., 2021; Fig. 10). Detrital zircon in the Snowcap assemblage in Yukon is dominated by a ca. 1850 Ma population with secondary peaks at ca. 1780 Ma, ca. 2000 Ma, ca. 2300 Ma, and ca. 2650 Ma (Fig. 10B). Late Mesoproterozoic zircon is rarely reported in the Snowcap assemblage and never forms a significant portion of the detrital zircon population. A rare late Neoproterozoic zircon peak is common to the Florence Range suite and the Snowcap assemblage (Figs. 10A and 10B).

Metamorphosed pre-Devonian siliciclastic rocks of the Tracy Arm assemblage form a narrow belt west of the Coast Mountains in SE Alaska and resemble the Snowcap assemblage (e.g., Gehrels et al., 1991; McClelland et al., 1992; Gareau and Woodsworth, 2000; Gehrels, 2000, 2001), although the presence of Late Ordovician through Early Devonian magmatism in SE Alaska may indicate that their origin and tectonic evolution may be somewhat

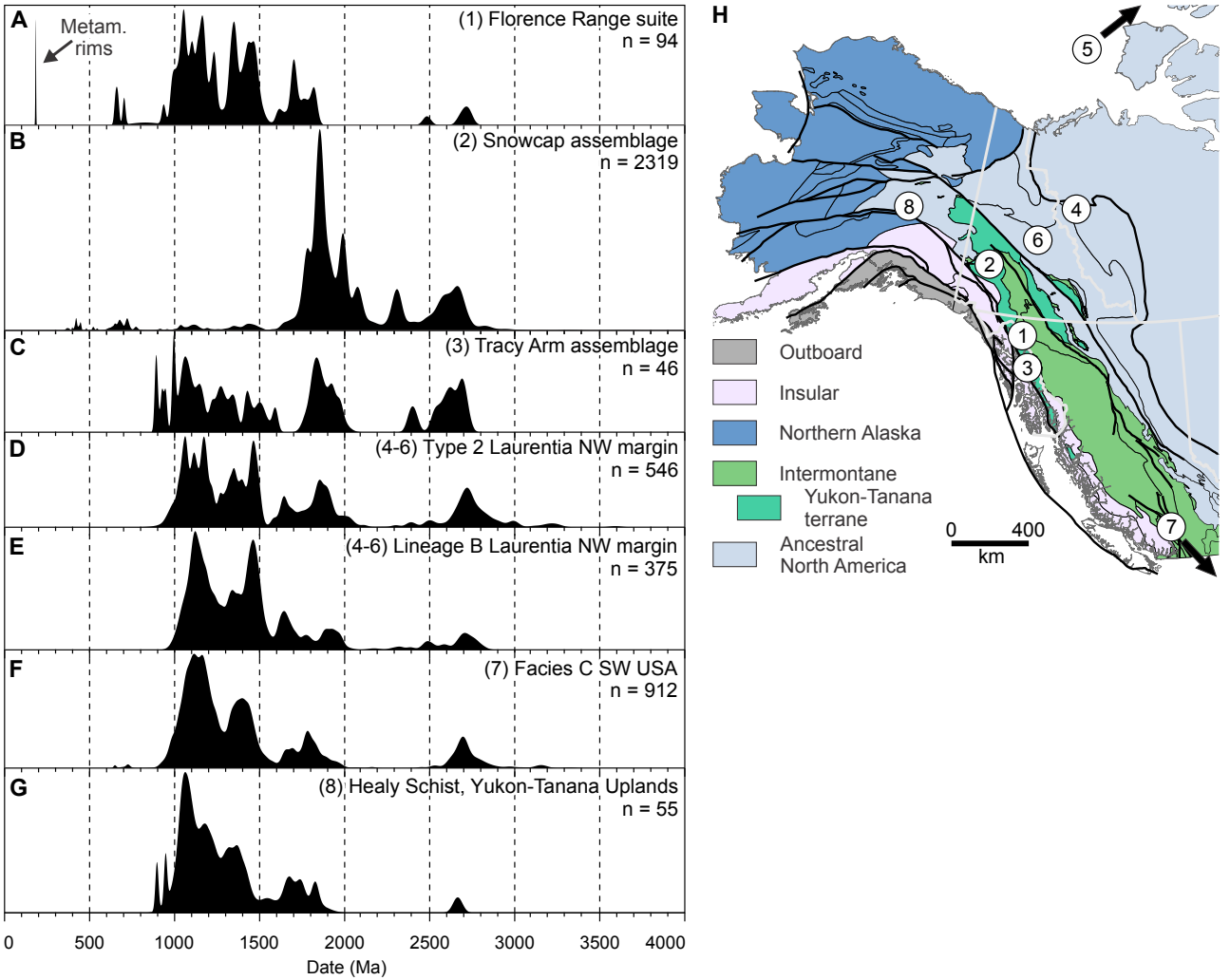

Figure 10. Comparison of normalized probability density plots of U-Pb detrital zircon from (A) the Florence Range suite (composite plots of samples 11ZE-1005 and 11ZE-1007; Kellett and Iraheta Muniz, 2019; this study); (B) the Snowcap assemblage in Yukon (Ryan et al., 2021); (C) the Tracy Arm assemblage (sample 87GC420 of Pecha et al., 2016; Gehrels et al., 1991); (D) Laurentia type 2 signature of the NW margin of Laurentia (Hadlari et al., 2012, and references therein); (E) lineage B of the NW margin of Laurentia (Lane and Gehrels, 2014; including data from Leslie, 2009; excluding data from Hadlari et al., 2012 [which are already included in part D]); (F) the Neoproterozoic Mutual Formation and Caddy Canyon Quartzite in Nevada, Utah, and Idaho, USA (facies C of Matthews et al., 2018; also including data from Yonkee et al., 2014; Gehrels and Pecha, 2014), and (G) the Healy Schist in the Yukon-Tanana Upland (sample 05ADb34 of Dusel-Bacon et al., 2017). Age interpretations are based on $^{206}Pb/^{238}U$ dates for dates younger than 1 Ga and $^{207}Pb/^{206}U$ dates for dates older than1 Ga. Only <10% discordant analyses are included, except where authors originally filtered their data set with stricter criteria. (H) Simplified map of first-order tectonic entities modified from Colpron and Nelson (2011) with approximate locations of detrital zircon populations discussed in the text and shown in parts A–G. 1—Florence Range; 2—Snowcap assemblage in Yukon; 3—Tracy Arm assemblage; 4—Mackenzie Mountains Supergroup; 5—Shaler Supergroup; 6—Windermere Supergroup; 7—Neoproterozoic sedimentary formations from southwest United States; 8—Healy Schist.

different from the Yukon-Tanana terrane (e.g., Saleeby, 2000; Pecha et al., 2016; Kroeger et al., 2023). A compilation of the detrital zircon dates from the Tracy Arm assemblage (n = 688; Pecha et al., 2016) reveals that the detrital zircon population is dominated by middle to late Paleoproterozoic zircon with a significant amount of late Mesoproterozoic zircon. However, this age peak is mainly derived from a single sample (87GC420, originally collected by Gehrels et al., 1991) in which the detrital zircon population is almost entirely Mesoproterozoic (Tables S2 and S4 in Pecha et al., 2016; Fig. 10C).

Late Mesoproterozoic detrital zircon in the Florence Range suite and in rare samples from SE Alaska (Gehrels et al., 1991; Pecha et al., 2016) indicates that the southwestern part of the Yukon-Tanana terrane had a distinct Grenvillian source that did not contribute zircon to the northern part of the Yukon-Tanana terrane (Saleeby, 2000; Pecha et al., 2016). As there are no Mesoproterozoic orogenic belts on the western margin of Laurentia, Mesoproterozoic zircon was likely recycled from sedimentary sources on the NW margin of Laurentia. These may include the early Neoproterozoic Mackenzie Mountains Supergroup and Shaler Supergroup (Sequence B of Young et al., 1979), the late Neoproterozoic Windermere Supergroup (Sequence C of Young et al., 1979), and the sedimentary units derived from these groups (Leslie, 2009; Laurentia type 2 signature of Hadlari et al., 2012; Lineage B of Lane and Gehrels, 2014; Figs. 10D and 10E). Several Neoproterozoic sedimentary formations from the southwest United States are also dominated by late Mesoproterozoic zircon and have secondary age peaks at ca. 1.4 Ga, ca. 1.7 Ga, and ca. 2.7 Ga (Facies C of Matthews et al., 2018; Gehrels and Pecha, 2014; Yonkee et al., 2014; Fig. 10F). Notably, pre-Carboniferous Grenville zircon–rich sedimentary units have not been identified in NW British Columbia, implying significant lateral transport of the southern part of the Yukon-Tanana terrane relative to its source region on Laurentia, or along-shore transport of detrital zircon.

Parautochthonous units of Ancestral North America in eastern Alaska (Yukon-Tanana Upland) are interpreted as stratigraphic equivalents to the Snowcap assemblage (e.g., Dusel-Bacon et al., 2006; Nelson et al., 2006) that remained attached to the Laurentian margin following the departure of the Yukon-Tanana terrane (Colpron et al., 2006a). They are characterized by Paleoproterozoic and older detrital zircon populations, but rare Mesoproterozoic grains have been reported in several samples, and one sample contained a dominant late Mesoproterozoic age peak (Healy schist; Dusel-Bacon et al., 2017; Fig. 10G). These units could therefore provide a tie between the Snowcap-equivalent strata in the southern part of the Yukon-Tanana terrane and the Laurentian margin in central and northern Yukon and eastern Alaska. If the southern part of the Yukon-Tanana terrane originated near the Yukon-Tanana Upland, it could have been transported to its current location along a NNW-striking sinistral strike-slip fault east of our study area (e.g., Pecha et al., 2016), similar to Late Jurassic to Early Cretaceous faults within and west of the Yukon-Tanana terrane (Monger et al., 1994; Chardon et al., 1999; Gehrels et al., 2009; Angen et al., 2014; Tochilin et al., 2014; Yokelson et al., 2015), and consistent with the Late Jurassic to Early Cretaceous sinistral oblique plate motion along the Cordilleran margin (Engebretson et al., 1985).

Comparison of the Boundary Ranges and Whitewater Suites with the Yukon-Tanana Terrane and the Stikine Assemblage

The Boundary Ranges suite has been correlated with the Yukon-Tanana terrane (Mihalynuk et al., 1999) and to the basement of the Stikine terrane (Stikine assemblage; Currie and Parrish, 1997). The Boundary Ranges suite amphibolite is older than a 369 ± 4 Ma to 367 ± 7 Ma orthogneiss unit (this study) and may have been coeval with the Ecstall magmatic cycle recognized in the Yukon-Tanana terrane, Alaska Range and Yukon-Tanana Upland (Fig. 11; 390–365 Ma; Piercey et al., 2006). The Ecstall cycle is generally characterized by bimodal magmatism. Felsic rocks range from calc-alkaline to peralkaline, whereas mafic rocks are characterized by OIB signatures, consistent with a continental rift setting (Dusel-Bacon et al., 2006; Piercey et al., 2006). Limited geochemical and isotopic data indicate that the Ecstall cycle magmatism in the Alaska Range and Coast Mountains of NW British Columbia and SE Alaska may have a continental arc affinity (Gehrels et al., 1992; Alldrick and Gallagher, 2000; Gareau and Woodsworth, 2000; Alldrick, 2001; Dashevsky et al., 2003). Because the geochemical characteristics of the Boundary Ranges suite amphibolite are consistent with a metasomatized mantle source related to an active or past subduction zone, our data suggest a correlation with this continental arc magmatism.

Currie and Parrish (1997) correlated the Boundary Ranges suite with the Paleozoic Stikine assemblage on the basis of lithological similarity and age of magmatism. The age of magmatism of the Boundary Ranges suite was previously constrained by variably discordant Late Devonian to Early Mississippian zircon dates (Currie and Parrish, 1997). Our new data indicate that the Boundary Ranges suite amphibolite cannot be younger than the Late Devonian, the age of crosscutting felsic orthogneiss (Fig. 11). The oldest units of the Stikine assemblage are poorly constrained and comprise minor Devonian volcano-sedimentary units and limestone that are intruded by the Forrest-Kerr plutonic suite (Fig. 11; Logan et al., 2000). Stikine assemblage tuff yielded a discordant Late Devonian U-Pb zircon date (380 ± 5 Ma; Logan et al., 2000). The Forrest Kerr plutonic suite yielded discordant Late Devonian U-Pb zircon dates (upper intercept 370.7 ± 6.7 Ma and 369.4 ± 5.1 Ma) and Mississippian Ar-Ar dates (343 ± 12 Ma and 346 ± 10 Ma) (Fig. 11; Logan et al., 2000), suggesting that parts of the Stikine assemblage may be coeval with the Boundary Ranges suite. However, the Stikine assemblage is characterized by abundant Mississippian–Pennsylvanian bimodal felsic and mafic volcanic rocks (340–310 Ma; Logan et al., 2000; Gunning et al., 2006; Nelson, 2017) and voluminous Carboniferous and Permian limestone (e.g., Gunning et al., 2007), intruded by Late Triassic plutonic rocks (e.g., Logan and Mihalynuk, 2014), which have not been identified in the Boundary Ranges suite (Fig. 11). The early Permian Stikine assemblage is generally characterized by carbonate sedimentation in a slope/ramp environment (e.g., Gunning et al., 1994; Logan et al., 2000). In contrast, the Boundary Ranges suite was metamorphosed in the early Permian (288 ± 7 Ma) and may have shared a similar tectonic evolution to the continental Florence Range suite since the Permian (Fig. 11; this study). Overall,

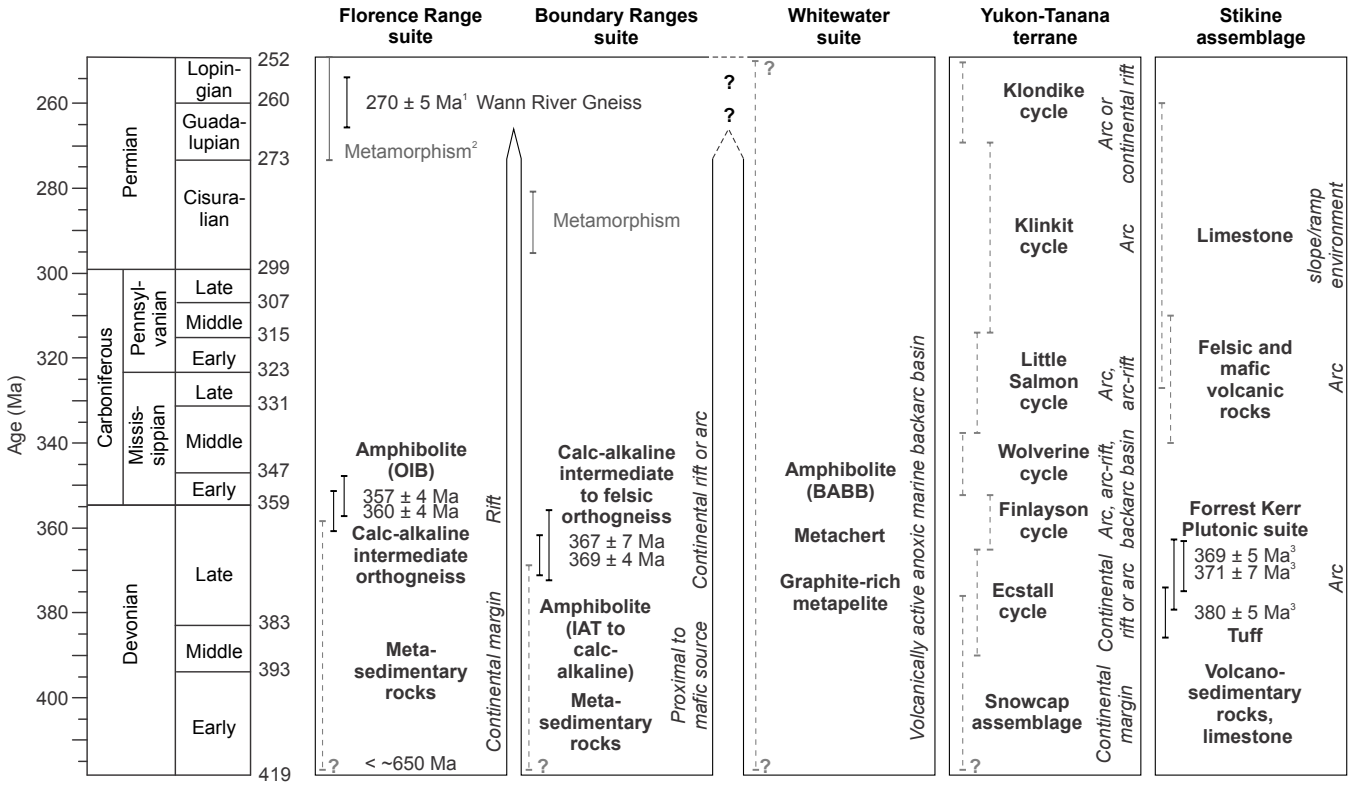

Figure 11. Comparison between the Florence Range, Boundary Ranges, and Whitewater suites (this study), the Yukon-Tanana terrane in Yukon (Piercey et al., 2006; Piercey and Colpron, 2009), and the Stikine assemblage (Logan et al., 2000; Gunning et al., 2006, 2007). Time scale is from Walker and Geissman (2022). Presumed Paleozoic or older age of the Whitewater suite is from Mihalynuk et al. (1994). U-Pb zircon geochronological data (solid lines) are from this study except: 1—Currie (1992a); 2—Soucy La Roche et al. (2022a); 3—Logan et al. (2020). Ages in Logan et al. (2020) are discordant upper-intercept dates. IAT—island-arc tholeiite; BABB—back-arc basin basalt; OIB—oceanic-island basalt.

distinctly different early Permian tectonic environments, the lack of evidence of similar Triassic magmatism, and the generally accepted juvenile character of the Late Triassic Stikine terrane indicate that the Stikine assemblage is not correlative to the Boundary Ranges suite. We therefore suggest that a correlation between the Boundary Ranges suite and part of the Yukon-Tanana terrane is most consistent with available data. The Yukon-Tanana terrane in this area was not juxtaposed with the Stikine terrane until the latest Triassic to Early Jurassic, as indicated by stitching magmatism (Minto, Long Lake, and Tagish suites; Mihalynuk et al., 1999; Colpron et al., 2016; Sack et al., 2020). This is consistent with the recent, latest Triassic–earliest Jurassic models of the collision of the Yukon-Tanana and Stikine terranes (George et al., 2021; Nelson et al., 2022; Ootes et al., 2022).

Previous interpretations of the Whitewater suite correlated it with the Boundary Ranges suite and with parts of the Yukon-Tanana terrane in Yukon (Mihalynuk et al., 1994). Whitewater suite geochemical characteristics indicate formation near a back-arc, a tectonic setting that is distinctly different from the Boundary Ranges suite (or the Stikine assemblage), and so these results preclude their direct correlation (cf. Mihalynuk et al., 1994). The Yukon-Tanana terrane in Yukon is internally variable and includes volcanic rocks with MORB or BABB geochemistry (e.g., Piercey et al., 2004, 2006; Nelson and Friedman, 2004; Devine et al., 2006) and piemontite-bearing chert (Piercey et al., 2004; Nelson and Friedman, 2004; Murphy et al., 2006; Mihalynuk et al., 2006). As such, the Whitewater suite may be correlative to parts of the Yukon-Tanana terrane, although the lack of age constraints on the Whitewater suite precludes correlation to specific units (Fig. 11).

Timing Constraints on Polymetamorphism

Our new U-Pb zircon geochronology data provide additional and new constraints on the timing of metamorphism in the Florence and Boundary Ranges suites. The main metamorphic event that affected both suites is earliest Jurassic Barrovian metamorphism that produced abundant prograde to peak monazite between 195 Ma and 185 Ma (Soucy La Roche et al., 2022a) and ca. 190–185 Ma garnet (Dyer, 2020) in the Florence Range suite, as well as ca. 200–190 Ma garnet in the Boundary Ranges suite (Dyer, 2020). This metamorphic event resulted in formation of Early Jurassic zircon grains and metamorphic overgrowths in the upper-amphibolite-facies Florence Range suite amphibolite and orthogneiss (low-precision Early Jurassic dates in sample 18ZE-R-33 and 187 ± 2 Ma weighted average date in sample 18ZE-R-35B) and quartzofeldspathic schist (183 ± 5 Ma date on a single zircon from sample 11ZE-1007). The Boundary Ranges suite does not preserve evidence for zircon (re-)crystallization, consistent with its lower metamorphic grade (lower amphibolite facies).

Soucy La Roche et al. (2022a) documented rare 270–240 Ma monazite and xenotime inclusions in garnet indicating cryptic Permian–Triassic prograde to peak metamorphism in the Florence Range suite. Several Permian zircon dates in sample 18ZE-R-35B and one slightly discordant Triassic date from a metamorphic overgrowth on detrital zircon in sample 11ZE-R-1005 support Permian–Triassic metamorphism of the Florence Range suite. Evidence of Permian metamorphism is also present in the Boundary Ranges suite. Zircon in orthogneiss sample 15ZE-1073 is commonly overgrown by thin (5–25 µm) CL-bright homogeneous to oscillatory zoned rims that yielded a 288 ± 7 Ma weighted average date (n = 5), which is interpreted as the best estimate for the age of metamorphic crystallization (Fig. 4C).

Our data indicate that the Florence Range and Boundary Ranges suites both record metamorphism during the Permian, with a time lag (ca. 270–240 Ma vs. ca. 288 Ma, respectively). Diachronous records of metamorphism are common within apparently continuous metamorphic units or sequences in other orogens around the world (e.g., Larson et al., 2013; Anczkiewicz et al., 2014; Briggs et al., 2018). This time lag between units with different protoliths that were metamorphosed at different metamorphic grades (upper vs. lower amphibolite facies) is compatible with a single tectonic event and may suggest a common tectonic evolution since the Permian. A similar time lag is present for the Early Jurassic metamorphism of these units, where the oldest garnet in the Florence Range suite is ~10 m.y. younger than the oldest garnet in the Boundary Ranges suite (Dyer, 2020). We therefore suggest that the Florence Range and Boundary Ranges suites interacted with each other since the Permian, even though they were likely located at different structural levels.

A shared evolution of the Florence Range and Boundary Ranges suites as early as the Permian indicates that the Wann River shear zone, which separates them, may be much older than Early Jurassic (cf. Currie and Parrish, 1993, 1997; Soucy La Roche et al., 2022b). Permian metamorphism of the Florence Range and Boundary Ranges suites is difficult to reconcile with the previous interpretation of the Wann River gneiss (270 ± 5 Ma; Currie, 1992a) as a metavolcanic unit deposited on top of the Boundary Ranges suite and later tectonically interlayered at the outcrop scale with metasedimentary units of the Florence Range suite (Currie and Parrish, 1997). It is more likely that the Wann River gneiss stitches the Florence Ranges and Boundary Ranges suites, and its finely banded texture is the product of shear-related grain-size reduction (Zagorevski et al., 2018).

The 288 ± 7 Ma metamorphic age in the Boundary Ranges suite is older than documented Permian metamorphic events in the Yukon-Tanana terrane (≤270 Ma; Creaser et al., 1997a; Philippot et al., 2001; Beranek and Mortensen, 2011; Petrie et al., 2016; Soucy La Roche et al., 2022a). However, Paleozoic metamorphism in the Yukon-Tanana terrane is generally sparsely constrained, and there may be significant diachroneity and differences in metamorphic conditions within each episode, especially considering the size of this terrane.

Tectonic Setting of the Paleozoic Yukon-Tanana Terrane and Modern Analogues

Geochemical and geochronological characteristics of the Florence Range, Boundary Ranges, and Whitewater suites in NW British Columbia could be produced in several unrelated or interrelated tectonic scenarios. Despite uncertainties related to paleogeography and tectonic relationships, there are modern analogues that can reconcile the seemingly disparate elements described herein. In this section, we use these modern analogues in the west and southwest Pacific Ocean to explore tectonic scenarios where these suites could have formed in genetically linked settings. These settings include the Japan arc–Sea of Japan back-arc–Korean Peninsula, Luzon arc–South China Sea, and Solomon arc–Woodlark Basin.

The Japan arc–Sea of Japan back-arc–Korean Peninsula system in the western Pacific Ocean formed during northwestward subduction of the Pacific and Philippine Sea plates under the Eurasian plate. It is composed, from SE to NW, of the Japan arc, the Sea of Japan back-arc basin, and the Eurasian continental margin in Korea, China, and Russia (Figs. 12A and 12B; see reviews in Taira, 2001; Yoshida et al., 2014; Van Horne et al., 2017). The Japan arc initially formed on Eurasian crust during the Paleocene–Oligocene prior to rifting and opening of the Sea of Japan during the early Miocene, followed by island-arc magmatism from the mid-Miocene to present (Yoshida et al., 2014). Magmatic and volcanic rocks with arc-like signatures and derived volcaniclastic sedimentary rocks occur in and close to the Japan arc. The Japan arc is now separated from the Eurasian margin by the Sea of Japan, which is in part underlain by MORB-like oceanic crust in the Yamato and Japan basins (Hirata et al., 1992; Hirahara et al., 2015). Finally, the Eurasian continental margin on the Korean Peninsula is composed of pre-Tertiary continental margin basement rocks and Tertiary sedimentary basins that host early Miocene volcanic rocks with arc compositions, and mid-Miocene and younger volcanic rocks with OIB compositions (Pouclet et al., 1994; Choi et al., 2006, 2013).

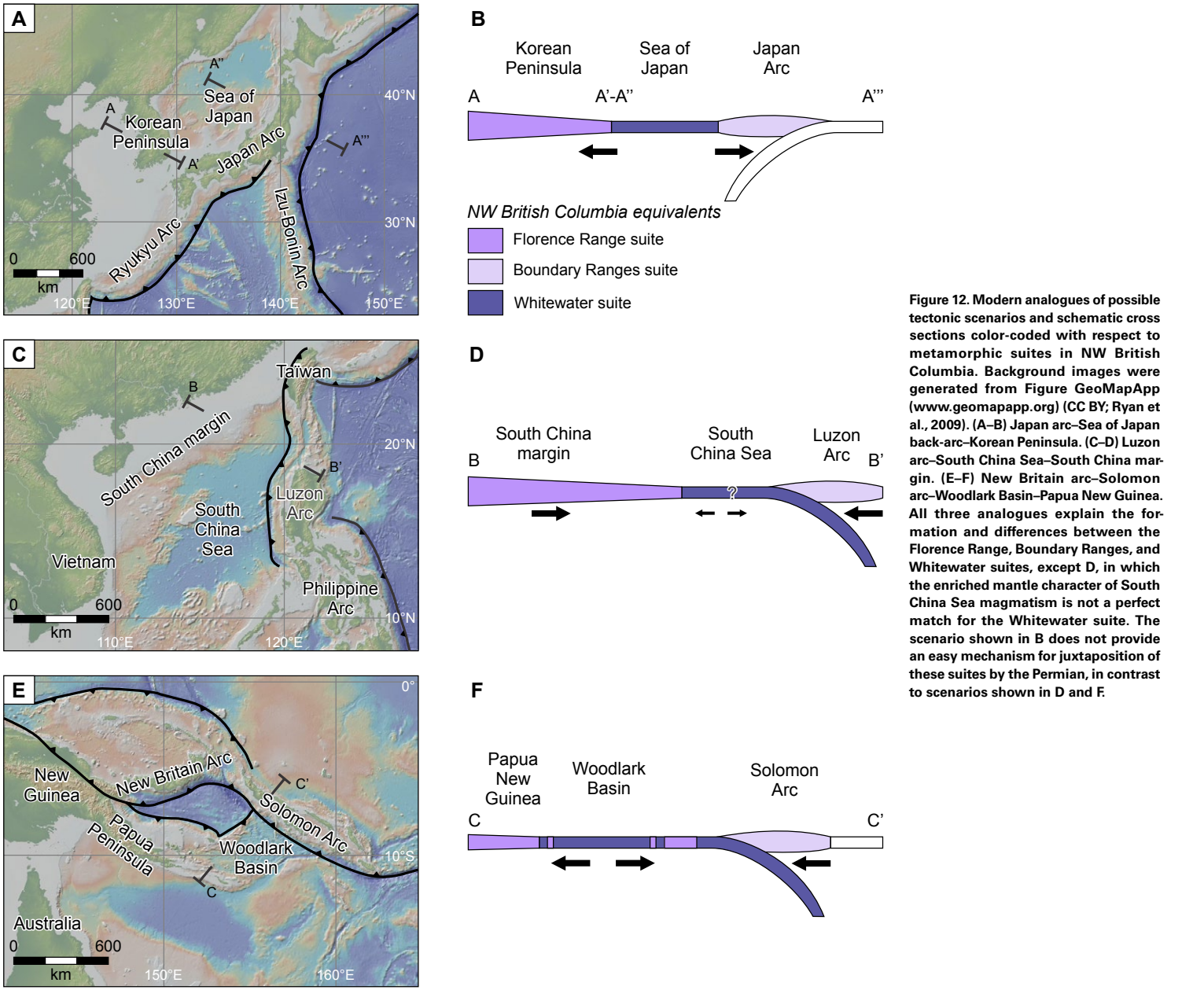

Figure 12. Modern analogues of possible tectonic scenarios and schematic cross sections color-coded with respect to metamorphic suites in NW British Columbia. Background images were generated from Figure GeoMapApp (www.geomapapp.org) (CC BY; Ryan et al., 2009). (A–B) Japan arc–Sea of Japan back-arc–Korean Peninsula. (C–D) Luzon arc–South China Sea–South China margin. (E–F) New Britain arc–Solomon arc–Woodlark Basin–Papua New Guinea. All three analogues explain the formation and differences between the Florence Range, Boundary Ranges, and Whitewater suites, except D, in which the enriched mantle character of South China Sea magmatism is not a perfect match for the Whitewater suite. The scenario shown in B does not provide an easy mechanism for juxtaposition of these suites by the Permian, in contrast to scenarios shown in D and F.

The Japan arc–Sea of Japan back-arc–Korean Peninsula system was previously proposed as an analogue to the Yukon-Tanana and Slide Mountain terranes in Yukon (e.g., Nelson, 1993; Creaser et al., 1997b; Piercey et al., 2004; Colpron et al., 2007; Colpron and Nelson, 2021) and may also explain the formation of the Florence Range, Boundary Ranges ,and Whitewater suites in a spatially contiguous tectonic system (Fig. 12B). Within the context of this analogue, the Florence Range suite metasedimentary rocks would be equivalent to the ancestral Eurasian margin, whereas Florence Range magmatism (360 ± 4 Ma calc-alkaline intermediate magmatic rocks and 357 ± 4 Ma mafic rocks with OIB composition) would be equivalent to mid-Miocene and younger rocks on the Korean Peninsula. As such, dated Florence Range magmatism formed on the passive margin of the back-arc basin. The Whitewater suite BABB mafic rocks, pelite, and chert could be equivalent to rocks in the Yamato and Japan basins. The presence of rare ultramafic rocks (Mihalynuk et al., 1994) could be a primary characteristic of the basin with ultramafic rocks exhumed along a ridge (e.g., MacLeod et al., 2009; Harigane et al., 2011) or related to accretion, where ultramafic rocks were preserved along the accretionary structures or related to serpentinite mélanges (e.g., Huang et al., 2018). The Boundary Ranges suite could be equivalent to the Japan arc or more likely to the Ryukyu arc along strike because Boundary Ranges metapelite and rare graphitic schist and marble are consistent with a submarine environment of deposition. The Japan arc–Sea of Japan back-arc–Korean Peninsula system provides an excellent analogue for the formation of the suites in NW British Columbia; however, it does not provide an easy mechanism for juxtaposition of the Florence Range and Boundary Ranges suites, and presumably the Whitewater suite, by the Permian. This would require initiation of subduction in the Whitewater basin between the Florence Range and Boundary Ranges suites, but there is no tectonic cause (e.g., arc-arc collision) for a subduction flip between the Early Mississippian and the Permian. Furthermore, there is no evidence for subduction-related magmatism in the Florence Range and Boundary Ranges suites that preceded their juxtaposition. Permian magmatism is restricted to the 270 ± 5 Ma Wann River gneiss (Currie, 1992a), which is younger than the 288 ± 7 Ma age of metamorphism in the Boundary Ranges suite.

Direct comparison of the NW British Columbia suites to the Yukon-Tanana and Slide Mountain terrane in Yukon is somewhat problematic because the arc, back-arc, and rift signatures are not well separated in the Yukon-Tanana terrane in Yukon, suggesting that the Yukon-Tanana terrane combines rocks that formed in different tectonic settings and were subsequently amalgamated (e.g., Parsons et al., 2018; Ryan et al., 2021). Superficially, the Whitewater suite may be equivalent to the Slide Mountain terrane; however, van Staal et al. (2018) and Parsons et al. (2019) demonstrated that parts of the Slide Mountain terrane are mid-Permian and therefore much too young to conform to the previously invoked Late Devonian Sea of Japan model. Similarly, although the Florence Range suite has been correlated to the Snowcap assemblage and likely the Grass Lakes suite, there is no evidence that the Florence Range suite became the basement to the Boundary Ranges arc, and the presence of OIB magmatism suggests that it became the passive margin of the back-arc basin in the Japan arc–Sea of Japan back-arc–Korean Peninsula analogue (Zagorevski et al., 2021). As such, the Florence Range suite may be a closer equivalent to the White River assemblage in western Yukon (Ryan et al., 2013, 2014, 2021) or the Healy schist in east-central Alaska (Dusel-Bacon et al., 2017), interpreted to be part of the parautochthonous margin of Laurentia, rather than the Snowcap assemblage, which forms the basement to a late Paleozoic arc.

The Luzon arc–South China Sea–South China margin system provides an alternate analogue for the Florence Range, Boundary Ranges, and Whitewater suites. It is composed, from east to west, of the Luzon arc, South China Sea, and Eurasian continental margin in South China and Vietnam (Figs. 12C and 12D; Juan et al., 1983; Defant et al., 1989; Yan et al., 2006). Major plate reorganization in the middle Miocene resulted in initiation of east-dipping subduction in the western Pacific and formation of the Luzon arc. Miocene rifting along the Asian margin resulted in opening of the South China Sea west of the Luzon arc, which has been linked to the India-Asia collision (e.g., Tapponnier et al., 1982; Leloup et al., 1995) or outboard subduction in the Pacific Ocean (e.g., Taylor and Hayes, 1980; Fyhn et al., 2009). Opening of the South China Sea resulted in Miocene and younger intraplate magmatism along the South China margin and ridge formation in the South China Sea (Chung et al., 1994). Continued eastward subduction of the South China Sea resulted in diachronous Luzon Arc–South China margin collision in Taiwan and continued oceanic subduction in the South China Sea (Huang et al., 2006). The collision in Taiwan juxtaposes intraplate magmatic rocks related to the opening of the South China Sea with coeval arc magmatic rocks in the Luzon arc. Within this analogue, the Florence Range suite would be equivalent to the South China Sea margin, and the Boundary Ranges suite would be equivalent to the Luzon arc and derived volcaniclastic sedimentary rocks (Fig. 12D). The South China Sea is analogous but not directly equivalent to the Whitewater suite, as magmatism in the South China Sea is characterized by enriched mantle (Chung et al., 1994). However, continental rifts can tap less enriched or previously metasomatized mantle, leading to BABB-like compositions (e.g., Robertson, 2007). A tectonic setting such as the Luzon arc–South China Sea can explain much of the differences between the Florence Range, Boundary Ranges, and Whitewater suites. In contrast to the Japan arc–Sea of Japan back-arc–Korean Peninsula analogue, the presence of a subduction zone between the South China margin and the Luzon arc provides a mechanism for their Permian juxtaposition (Fig. 12B vs. Fig. 12D). In this case, continued subduction of the South China Sea (Whitewater suite) juxtaposed the Luzon arc (Boundary Ranges suite) with the South China margin (Florence Range suite). The Whitewater suite may have been offscraped and incorporated into an accretionary prism during subduction. The absence of Late Mississippian to early Permian arc rocks in the Boundary Ranges suite, which would be expected from continuous subduction beneath a Boundary Ranges arc, is less problematic with this model. Basement of forearcs, which are in more direct contact with the subducting plate and colliding margins, can be significantly older than active arcs (e.g., Falloon et al., 2014; Reagan et al., 2019). It is thus possible that the Boundary Ranges suite represents the forearc of a Late Mississippian to early Permian arc that may

not be preserved in NW British Columbia. Magmatic rocks of that age are present in other parts of the Yukon-Tanana terrane (e.g., Piercey et al., 2006)

Last, the Solomon arc–New Britain arc–Woodlark Basin–Papua New Guinea system provides a similar analogue for the Florence Range, Boundary Ranges, and Whitewater suites. The Australian plate subducts northward beneath the New Britain and Solomon arcs and contains an active rift, the Woodlark Basin (Figs. 12E and 12F; see reviews in Baldwin et al., 2012; Weissel et al., 1982). This rift is propagating into the Papuan Peninsula (part of the Australian plate), resulting in magmatism with highly variable composition along the rift, ranging from tholeiitic to calc-alkaline (Perfit et al., 1987; Stolz et al., 1993; Park et al., 2018). Alkaline basalts with OIB compositions are present in New Guinea (Richards et al., 1990). In principle, Papua New Guinea and the Woodlark Basin could explain the Florence Range suite and the Boundary Ranges and Whitewater suites, respectively. However, the arc-like rocks of the Boundary Ranges suite may also be equivalent to the New Britain arc or Solomon arc (e.g., Woodhead and Johnson, 1993; Petterson et al., 2011). Incorporation of elements of the Woodlark Basin (Whitewater suite) into the accretionary prism and eventual collision of the New Britain and Solomon arcs (Boundary Ranges suite) with the Papuan Peninsula (Florence Range suite) would juxtapose all three suites together. The absence of Late Mississippian to early Permian arc rocks is explained similarly as for the Luzon arc–South China Sea–South China margin analogue.

The three modern analogues explain most or all of the geochemical and geochronological characteristics of the Florence Range, Boundary Ranges, and Whitewater suites in NW British Columbia and the tectonic processes leading to their juxtaposition. The Japan arc–Sea of Japan back-arc–Korean Peninsula is an excellent analogue to explain the geochemical characteristics of the suites, but it fails to provide a juxtaposition mechanism. A difference in the subduction location and polarity, such as in the Luzon arc–South China Sea scenario, provides such a mechanism, but the geochemical characteristics of the rocks therein do not match perfectly those of the three NW British Columbia suites. Finally, the Papua New Guinea–New Britain arc–Solomon arc–Woodlark Basin analogue explains both the geochemical characteristics of the rocks and provides a tectonic mechanism for their juxtaposition. Other tectonic scenarios may explain the origin and tectonic evolution of the Florence Range, Boundary Ranges, and Whitewater suites. For example, the role of transcurrent motion is not considered in the modern analogues for simplicity. There is evidence for Late Jurassic to Early Cretaceous sinistral-sense motion and Late Cretaceous to Quaternary dextral-sense motion (Monger et al., 1994; Chardon et al., 1999; Gabrielse et al., 2006; Gehrels et al., 2009; Angen et al., 2014; Tochilin et al., 2014; Yokelson et al., 2015; Monger and Gibson, 2019), but transcurrent motion during the Paleozoic is not constrained precisely enough to be integrated in models. Younger local structures, such as the Wann River shear zone, add further uncertainty to the original position of the metamorphic suites, which may not have formed perfectly aligned across-strike. Restoration of displacement associated with this shear zone is currently not possible, given its polyphase evolution and the lack of constraints on the amount of displacement (Soucy La Roche et al., 2022b). In any case, it is clear that the Yukon-Tanana terrane is composed of multiple packages of rocks that originated in distinct but possibly genetically linked settings. A thorough characterization of the ages and chemical compositions of lithological suites within the terrane, and in contact with the terrane, can help to elucidate the complex tectonic and magmatic processes that led to its formation. A better understanding of the structures that separate segments of the Yukon-Tanana terrane that have distinct origins is a logical next step to understand its assembly (e.g., Parsons et al., 2018).

CONCLUSIONS

Our new geochronological and immobile trace-element geochemical data indicate that the Florence Range, Boundary Ranges, and Whitewater metamorphic suites in NW British Columbia were formed in distinct tectonic settings and were subsequently amalgamated into the Yukon-Tanana terrane. In the Florence Range suite, late Neoproterozoic or younger to pre–latest Devonian continental margin metasedimentary rocks (metamorphosed pelite, psammite, quartz arenite, carbonate, and rare chert) were intruded by 360 ± 4 Ma calc-alkaline intermediate orthogneiss and 357 ± 4 Ma amphibolite with OIB composition in a continental rift tectonic setting. In the Boundary Ranges suite, Late Devonian or older metasedimentary rocks were derived in part from a mafic source, and the composition of interlayered amphibolite is consistent with a subduction-zone metasomatized mantle source. The Boundary Ranges suite also includes 369 ± 4 Ma to 367 ± 7 Ma calc-alkaline felsic to intermediate orthogneiss that has a composition compatible with multiple tectonic settings, including a continental volcanic arc or continental rift. In strong contrast, the Whitewater suite comprises manganiferous meta-chert, graphite-rich metapelite, and amphibolite with BABB composition, which is consistent with its formation in an anoxic basin near a volcanic source (e.g., spreading center or guyot). Differences in lithological and chemical compositions between the Florence Range and Boundary Ranges suites indicate that they were separate until at least the Early Mississippian, but the lack of robust geochronological constraints on the Whitewater suite hinders the assessment of its relationship with the two other metamorphic suites. The Florence Range and Boundary Ranges suites both record evidence of metamorphism during the Permian, which may indicate that they started to interact with each other at that time. The detrital signature of metasedimentary rocks from the Florence Range suite is dominated by late Mesoproterozoic zircon, which is rare or absent from coeval strata of the Snowcap assemblage in Yukon, and therefore suggests a distinct source. Overall, our study demonstrates that there are important lithological, geochemical, and provenance variations in pre-Mississippian strata at the scale of the Yukon-Tanana terrane, and even at the scale of relatively small regions such as the Atlin area in NW British Columbia. Intraterrane shear zones such as the Wann River shear zone likely added a lot of complexity to the distribution of rocks that formed in originally different tectonic settings and are now included in the Yukon-Tanana terrane. Comparison with modern analogues helps to understand the tectonic settings in which these rocks may have formed.

ACKNOWLEDGMENTS

We thank Sabastien Dyer for field assistance. Raymond Chung, Ron Christie, and Greg Case helped with mineral separation for U-Pb geochronology, and Pat Hunt helped with cathodoluminescence and backscattered-electron imaging of zircon. Tom Pestaj, Bill Davis, and Nicole Rayner assisted N. Joyce with sensitive high-resolution ion microprobe analytical work and carried out data reduction. Thomas Hadlari shared his compiled detrital zircon data. Lisel Currie supplied unpublished first-hand documentation about the geology of the Atlin area and provided comments on the manuscript. We thank journal reviewers Sean Reagan and Jamey Jones, Associate Editor Mark Holland, and Science Editor Christopher Spencer. Norm Graham of Discovery Helicopters provided reliable transportation to the field area. This manuscript is Natural Resources Canada contribution 20230113. This research was funded by the Geological Survey of Canada, Natural Resources Canada Geo-Mapping for Energy and Minerals Program (GEM-II) Cordillera project. All data generated or analyzed during this study are included in this paper and the Supplemental Material.

REFERENCES CITED

Alldrick, D.J., 2001, Geology and mineral deposits of the Ecstall greenstone belt, northwest British Columbia (NTS 103H/103I), *in* British Columbia Ministry of Energy and Mines Geological Fieldwork 2000: British Columbia Geological Survey Paper 2001–01, p. 279–306.

Alldrick, D.J., and Gallagher, C.S., 2000, Geology and mineral potential of the Ecstall VMS belt (NTS 103H, 103I), *in* British Columbia Ministry of Energy and Mines Geological Fieldwork 1999: British Columbia Geological Survey Paper 2000–01, p. 249–266.

Anczkiewicz, R., Chakraborty, S., Dasgupta, S., Mukhopadhyay, D., and Kołtonik, K., 2014, Timing, duration and inversion of prograde Barrovian metamorphism constrained by high resolution Lu-Hf garnet dating: A case study from the Sikkim Himalaya, NE India: Earth and Planetary Science Letters, v. 407, p. 70–81, https://doi.org/10.1016/j.epsl.2014.09.035.

Angen, J.J., Van Staal, C.R., Lin, S., Nelson, J.L., Mahoney, J.B., Davis, D.W., and McClelland, W.C., 2014, Kinematics and timing of shear zone deformation in the western Coast belt: Evidence for mid-Cretaceous orogen-parallel extension: Journal of Structural Geology, v. 68, p. 273–299, https://doi.org/10.1016/j.jsg.2014.05.026.

Baldwin, S.L., Fitzgerald, P.G., and Webb, L.E., 2012, Tectonics of the New Guinea region: Annual Review of Earth and Planetary Sciences, v. 40, p. 495–520, https://doi.org/10.1146/annurev-earth-040809-152540.

Beranek, L.P., and Mortensen, J.K., 2011, The timing and provenance record of the late Permian Klondike orogeny in northwestern Canada and arc-continent collision along western North America: Tectonics, v. 30, no. 5, TC5017, https://doi.org/10.1029/2010TC002849.

Berman, R.G., Ryan, J.J., Gordey, S.P., and Villeneuve, M., 2007, Permian to Cretaceous polymetamorphic evolution of the Stewart River region, Yukon-Tanana terrane, Yukon, Canada: *P-T* evolution linked with in situ SHRIMP monazite geochronology: Journal of Metamorphic Geology, v. 25, no. 7, p. 803–827, https://doi.org/10.1111/j.1525-1314.2007.00729.x.

Bhatia, M.R., and Crook, K.A., 1986, Trace element characteristics of graywackes and tectonic setting discrimination of sedimentary basins: Contributions to Mineralogy and Petrology, v. 92, no. 2, p. 181–193, https://doi.org/10.1007/BF00375292.

Bonazzi, P., and Menchetti, S., 2004, Manganese in monoclinic members of the epidote group: piemontite and related minerals: Reviews in Mineralogy and Geochemistry, v. 56, p. 495–552, https://doi.org/10.2138/gsrmg.56.1.495.

Briggs, S.I., Cottle, J.M., and Smit, M.A., 2018, Record of plate boundary metamorphism during Gondwana breakup from Lu-Hf garnet geochronology of the Alpine Schist, New Zealand: Journal of Metamorphic Geology, v. 36, no. 7, p. 821–841, https://doi.org/10.1111/jmg.12313.

Brown, D., Ryan, P.D., Afonso, J.C., Boutelier, D., Burg, J.P., Byrne, T., Calvert, A., Cook, F., DeBari, S., Dewey, J.F., and Gerya, T.V., 2011, Arc-continent collision: The making of an orogen: Berlin, Springer, p. 477–493, https://doi.org/10.1007/978-3-540-88558-0_17.

Cabanis, B., and Lecolle, M., 1989, Le diagramme La/10-Y/15-Nb/8: Un outil pour la discrimination des séries volcaniques et la mise en évidence des processus de mélange et/ou de contamination crustale: Comptes Rendus de l'Académie des Sciences, ser. 2, Mécanique, Physique, Chimie, Sciences de l'Univers, Sciences de la Terre, v. 309, no. 20, p. 2023–2029.

Canil, D., Johnston, S.T., Evers, K., Shellnutt, J.G., and Creaser, R.A., 2003, Mantle exhumation in an early Paleozoic passive margin, northern Cordillera, Yukon: The Journal of Geology, v. 111, no. 3, p. 313–327, https://doi.org/10.1086/373971.

Cann, J.R., 1970, Rb, Sr, Y, Zr and Nb in some ocean floor basaltic rocks: Earth and Planetary Science Letters, v. 10, no. 1, p. 7–11, https://doi.org/10.1016/0012-821X(70)90058-0.

Cawood, P.A., Kröner, A., Collins, W.J., Kusky, T.M., Mooney, W.D., and Windley, B.F., 2009, Accretionary orogens through Earth history, *in* Cawood, P.A., and Kröner, A., eds., Earth Accretionary Systems in Space and Time: Geological Society, London, Special Publication 318, p. 1–36, https://doi.org/10.1144/SP318.1.

Chardon, D., Andronicos, C.L., and Hollister, L.S., 1999, Large-scale transpressive shear zone patterns and displacements within magmatic arcs: The Coast Plutonic Complex, British Columbia: Tectonics, v. 18, no. 2, p. 278–292, https://doi.org/10.1029/1998TC900035.

Choi, H.O., Choi, S.H., Lee, D.C., and Kang, H.C., 2013, Geochemical evolution of basaltic volcanism within the Tertiary basins of southeastern Korea and the opening of the East Sea (Sea of Japan): Journal of Volcanology and Geothermal Research, v. 249, p. 109–122, https://doi.org/10.1016/j.jvolgeores.2012.09.007.

Choi, S.H., Mukasa, S.B., Kwon, S.T., and Andronikov, A.V., 2006, Sr, Nd, Pb and Hf isotopic compositions of late Cenozoic alkali basalts in South Korea: Evidence for mixing between the two dominant asthenospheric mantle domains beneath East Asia: Chemical Geology, v. 232, no. 3–4, p. 134–151, https://doi.org/10.1016/j.chemgeo.2006.02.014.

Chung, S.L., Sun, S.S., Tu, K., Chen, C.H., and Lee, C.Y., 1994, Late Cenozoic basaltic volcanism around the Taiwan Strait, SE China: Product of lithosphere-asthenosphere interaction during continental extension: Chemical Geology, v. 112, no. 1–2, p. 1–20, https://doi.org/10.1016/0009-2541(94)90101-5.

Cleven, N.R., Ryan, J.J., Kellett, D.A., Zagorevski, A., McClelland, B., Joyce, N.L., Crowley, J., and Parsons, A., 2019, Detrital-zircon age-distribution correlations between Snowcap assemblage basement of the Yukon-Tanana terrane and Proterozoic to Devonian stratigraphy of the Laurentian margin platformal strata, Yukon–British Columbia: Geological Survey of Canada Scientific Presentation 113, 1 poster, https://doi.org/10.4095/321395.

Colpron, M., and Nelson, J.L., 2011, A Digital Atlas of Terranes for the Northern Cordillera: British Columbia Ministry of Energy and Mines, British Columbia Geological Survey/Yukon Geological Survey GeoFile 2011-11, http://data.geology.gov.yk.ca/Compilation/2#InfoTab.

Colpron, M., and Nelson, J.L., 2021, Northern Cordillera: Canada and Alaska, *in* Alderton, D., and Elias, S.C., eds., Encyclopedia of Geology (2nd ed.): San Diego, California, Academic Press, p. 93–106.

Colpron, M., Nelson, J.L., and Murphy, D.C., 2006a, A tectonostratigraphic framework for the pericratonic terranes of the northern Cordillera, *in* Colpron, M., and Nelson, J.L., eds., Paleozoic Evolution and Metallogeny of Pericratonic Terranes at the Ancient Pacific Margin of North America, Canadian and Alaskan Cordillera: Geological Association of Canada Special Paper 45, p. 1–23.

Colpron, M., Mortensen, J.K., Gehrels, G.E., and Villeneuve, M.E., 2006b, Basement complex, Carboniferous magmatism and Paleozoic deformation in Yukon-Tanana terrane of central Yukon: Field, geochemical and geochronological constraints from Glenlyon map area, *in* Colpron, M., and Nelson, J.L., eds., Paleozoic Evolution and Metallogeny of Pericratonic Terranes at the Ancient Pacific Margin of North America, Canadian and Alaskan Cordillera: Geological Association of Canada Special Paper 45, p. 131–151.

Colpron, M., Nelson, J.L., and Murphy, D.C., 2007, Northern Cordilleran terranes and their interactions through time: GSA Today, v. 17, no. 4–5, p. 4–10, https://doi.org/10.1130/GSAT01704-5A.1.

Colpron, M., Crowley, J.L., Gehrels, G., Long, D.G., Murphy, D.C., Beranek, L., and Bickerton, L., 2015, Birth of the northern Cordilleran orogen, as recorded by detrital zircons in Jurassic synorogenic strata and regional exhumation in Yukon: Lithosphere, v. 7, no. 5, p. 541–562, https://doi.org/10.1130/L451.1.

Colpron, M., Israel S., and Friend M., 2016, Yukon Plutonic Suites: Yukon Geological Survey Open File 2016–37, scale 1:750,000.

Colpron, M., Sack, P.J., Crowley, J.L., Beranek, L.P., and Allan, M.M., 2022, Late Triassic to Jurassic magmatic and tectonic evolution of the Intermontane terranes in Yukon, northern Canadian Cordillera: Transition from arc to syn-collisional magmatism and post-collisional lithospheric delamination: Tectonics, v. 41, no. 2, https://doi.org/10.1029/2021TC007060.

Condie, K.C., Hatcher, R.D., Carlson, M.P., and McBride, J.H., 2007, Accretionary Orogens in Space and Time: Geological Society of America Memoir 200, 145 p., https://doi.org/10.1130/2007.1200(09).

Coney, P.J., Jones, D.L., and Monger, J.W., 1980, Cordilleran suspect terranes: Nature, v. 288, no. 5789, p. 329–333, https://doi.org/10.1038/288329a0.

Corfu, F., Hanchar, J.M., Hoskin, P.W., and Kinny, P., 2003, Atlas of zircon textures: Reviews in Mineralogy and Geochemistry, v. 53, no. 1, p. 469–500, https://doi.org/10.2113/0530469.

Creaser, R.A., Heaman, L.M., and Erdmer, P., 1997a, Timing of high-pressure metamorphism in the Yukon-Tanana terrane, Canadian Cordillera: Constraints from U-Pb zircon dating of eclogite from the Teslin tectonic zone: Canadian Journal of Earth Sciences, v. 34, no. 5, p. 709–715, https://doi.org/10.1139/e17-057.

Creaser, R.A., Erdmer, P., Stevens, R.A., and Grant, S.L., 1997b, Tectonic affinity of Nisutlin and Anvil assemblage strata from the Teslin tectonic zone, northern Canadian Cordillera: Constraints from neodymium isotope and geochemical evidence: Tectonics, 16, no. 1, p. 107–121, https://doi.org/10.1029/96TC03317.

Cui, Y., Miller, D., Schiarizza, P., and Diakow, L.J., 2017, British Columbia Digital Geology: British Columbia Ministry of Energy, Mines and Petroleum Resources, British Columbia Geological Survey Open File 2017–8, 9 p., data version 2019–12–19.

Currie, L.D., 1990, Metamorphic rocks in the Florence Range, Coast Mountains, northwestern British Columbia (104M/8), *in* British Columbia Ministry of Energy, Mines and Petroleum Resources Geological Fieldwork 1989: British Columbia Geological Survey Paper 1990–1, p. 197–203.

Currie, L.D., 1991, Geology of the Tagish Lake area, northern Coast Mountains, northwestern British Columbia, *in* Current Research, Part A: Geological Survey of Canada Paper 91–1A, p. 147–154, https://doi.org/10.4095/132508.

Currie, L.D., 1992a, Metamorphic rocks in the Tagish Lake area, northern Coast Mountains, British Columbia: A possible link between Stikinia and parts of the Yukon-Tanana terrane, *in* Current Research, Part E: Geological Survey of Canada Paper 92–1E, p. 199–208, https://doi.org/10.4095/132806.

Currie, L., 1992b, U-Pb geochronology of Cretaceous and Tertiary plutonic rocks of the Tagish Lake area, northeastern Coast Mountains, British Columbia, *in* Radiogenic Age and Isotopic Studies, Report 6: Geological Survey of Canada Paper 92–2, p. 163–170, https://doi.org/10.4095/134178.

Currie, L.D., 1994, The Geology and Mid-Jurassic Amalgamation of Tracy Arm Terrane and Stikinia of Northwestern British Columbia [Ph.D. thesis]: Ottawa, Ontario, Canada, Carleton University, 385 p., https://doi.org/10.22215/etd/1994-02875.

Currie, L.D., and Parrish, R.R., 1993, Jurassic accretion of Nisling terrane along the western margin of Stikinia, Coast Mountains, northwestern British Columbia: Geology, v. 21, no. 3, p. 235–238, https://doi.org/10.1130/0091-7613(1993)021<0235:JAONTA>2.3.CO;2.

Currie, L.D., and Parrish, R.R., 1997, Paleozoic and Mesozoic rocks of Stikinia exposed in northwestern British Columbia: Implications for correlations in the northern Cordillera: Geological Society of America Bulletin, v. 109, no. 11, p. 1402–1420, https://doi.org/10.1130/0016-7606(1997)109<1402:PAMROS>2.3.CO;2.

Dashevsky, S.S., Schaefer, C.F., and Hunter, E.N., 2003, Bedrock Geologic Map of the Delta Mineral Belt, Tok Mining District, Alaska: Alaska Division of Geological & Geophysical Surveys Professional Report 122, 122 p., https://doi.org/10.14509/2923.

Defant, M.J., Jacques, D., Maury, R.C., de Boer, J., and Joron, J.L., 1989, Geochemistry and tectonic setting of the Luzon arc, Philippines: Geological Society of America Bulletin, v. 101, no. 5, p. 663–672, https://doi.org/10.1130/0016-7606(1989)101<0663:GATSOT>2.3.CO;2.

Devine, F., Carr, S.D., Murphy, D.C., Davis, W.J., Smith, S., Villeneuve, M.E., Colpron, M., and Nelson, J.L., 2006, Geochronological and geochemical constraints on the origin of the Klatsa metamorphic complex: Implications for Early Mississippian high-pressure metamorphism within Yukon-Tanana terrane, *in* Colpron, M., and Nelson, J.L., eds., Paleozoic Evolution and Metallogeny of Pericratonic Terranes at the Ancient Pacific Margin of North America, Canadian and Alaskan Cordillera: Geological Association of Canada Special Paper 45, p. 107–130.

Dickinson, W.R., 2008, Impact of differential zircon fertility of granitoid basement rocks in North America on age populations of detrital zircons and implications for granite petrogenesis: Earth and Planetary Science Letters, v. 275, no. 1–2, p. 80–92, https://doi.org/10.1016/j.epsl.2008.08.003.

Dusel-Bacon, C., and Cooper, K.M., 2000, Trace-element geochemistry of metabasaltic rocks from the Yukon-Tanana Upland and implications for the origin of tectonic assemblages in east-central Alaska: Canadian Journal of Earth Sciences, v. 36, no. 10, p. 1671–1695, https://doi.org/10.1139/e99-077.

Dusel-Bacon, C., Wooden, J.L., and Hopkins, M.J., 2004, U-Pb zircon and geochemical evidence for bimodal mid-Paleozoic magmatism and syngenetic base-metal mineralization in the Yukon-Tanana terrane, Alaska: Geological Society of America Bulletin, v. 116, no. 7–8, p. 989–1015, https://doi.org/10.1130/B25342.1.

Dusel-Bacon, C., Hopkins, M.J., Mortensen, J.K., Dashevsky, S.S., Bressler, J.R., Day, W.C., Colpron, M., and Nelson, J.L., 2006, Paleozoic tectonic and metallogenic evolution of the pericratonic rocks of east-central Alaska and adjacent Yukon, *in* Colpron, M., and Nelson, J.L., eds., Paleozoic Evolution and Metallogeny of Pericratonic Terranes at the Ancient Pacific Margin of North America, Canadian and Alaskan Cordillera: Geological Association of Canada Special Paper 45, p. 25–74.

Dusel-Bacon, C., Holm-Denoma, C.S., Jones, J.V., Aleinikoff, J.N., and Mortensen, J.K., 2017, Detrital zircon geochronology of quartzose metasedimentary rocks from parautochthonous North America, east-central Alaska. Lithosphere, v. 9, p. 927–952, https://doi.org/10.1130/L672.1.

Dyer, S.C., 2020, The Early Jurassic Metamorphic History of the Yukon-Tanana Terrane of Northwestern British Columbia: Insights from a New Inverse Garnet Fractionation Modelling Technique [M.Sc. thesis]: Ottawa, Ontario, Canada, Carleton University, 314 p., https://doi.org/10.22215/etd/2020-14186.

Engebretson, D.C., Cox, A., and Gordon, R.G., 1985, Relative motions between oceanic and continental plates in the Pacific basin, *in* Engebretson, D.C., et al., eds., Relative Motions Between Oceanic and Continental Plates in the Pacific Basin: Geological Society of America Special Paper 206, p. 1–59, https://doi.org/10.1130/SPE206-p1.

Erdmer, P., Ghent, E.D., Archibald, D.A., and Stout, M.Z., 1998, Paleozoic and Mesozoic high-pressure metamorphism at the margin of ancestral North America in central Yukon: Geological Society of America Bulletin, v. 110, no. 5, p. 615–629, https://doi.org/10.1130/0016-7606(1998)110<0615:PAMHPM>2.3.CO;2.

Falloon, T.J., Meffre, S., Crawford, A.J., Hoernle, K., Hauff, F., Bloomer, S.H., and Wright, D.J., 2014, Cretaceous fore-arc basalts from the Tonga arc: Geochemistry and implications for the tectonic history of the SW Pacific: Tectonophysics, v. 630, p. 21–32, https://doi.org/10.1016/j.tecto.2014.05.007.

Fyhn, M.B., Boldreel, L.O., and Nielsen, L.H., 2009, Geological development of the Central and South Vietnamese margin: Implications for the establishment of the South China Sea, Indochinese escape tectonics and Cenozoic volcanism: Tectonophysics, v. 478, no. 3–4, p. 184–214, https://doi.org/10.1016/j.tecto.2009.08.002.

Gabrielse, H., Murphy, D.C., and Mortensen, J.K., 2006, Cretaceous and Cenozoic dextral orogen-parallel displacements, magmatism and paleogeography, north-central Canadian Cordillera, *in* Haggart, J., Enkin, R., and Monger, J.W.H., eds., Paleogeography of the North American Cordillera: Evidence For and Against Large-Scale Displacements: Geological Association of Canada Special Paper 46, p. 255–276.

Gaidies, F., Morneau, Y.E., Petts, D.C., Jackson, S.E., Zagorevski, A., and Ryan, J.J., 2021, Major and trace element mapping of garnet: Unravelling the conditions, timing and rates of metamorphism of the Snowcap assemblage, west-central Yukon: Journal of Metamorphic Geology, v. 39, no. 2, p. 133–164, https://doi.org/10.1111/jmg.12562.

Gareau, S.A., and Woodsworth, G.J., 2000, Yukon-Tanana terrane in the Scotia-Quaal belt, Coast Plutonic Complex, central-western British Columbia, *in* Stowell, H.H., and McClelland, W.C., eds., Tectonics of the Coast Mountains in SE Alaska and Coastal British Columbia: Geological Society of America Special Paper 343, p. 23–43, https://doi.org/10.1130/0-8137-2343-4.23.

Gehrels, G.E., 2000, Reconnaissance geology and U-Pb geochronology of the western flank of the Coast Mountains between Juneau and Skagway, southeastern Alaska, *in* Stowell, H.H., and McClelland, W.C., eds., Tectonics of the Coast Mountains in SE Alaska and Coastal British Columbia: Geological Society of America Special Paper 343, p. 213–234, https://doi.org/10.1130/0-8137-2343-4.213.

Gehrels, G.E., 2001, Geology of the Chatham Sound region, southeast Alaska and coastal British Columbia: Canadian Journal of Earth Sciences, v. 38, no. 11, p. 1579–1599, https://doi.org/10.1139/e01-040.

Gehrels, G., and Pecha, M., 2014, Detrital zircon U-Pb geochronology and Hf isotope geochemistry of Paleozoic and Triassic passive margin strata of western North America: Geosphere, v. 10, no. 1, p. 49–65, https://doi.org/10.1130/GES00889.1.

Gehrels, G.E., McClelland, W.C., Samson, S.D., and Patchett, P.J., 1991, U-Pb geochronology of detrital zircons from a continental margin assemblage in the northern Coast Mountains, southeastern Alaska: Canadian Journal of Earth Sciences, v. 28, no. 8, p. 1285–1300, https://doi.org/10.1139/e91-114.

Gehrels, G.E., McClelland, W.C., Samson, S.D., Patchett, P.J., and Orchard, M.J., 1992, Geology of the western flank of the Coast Mountains between Cape Fanshaw and Taku Inlet, southeastern Alaska: Tectonics, v. 11, no. 3, p. 567–585, https://doi.org/10.1029/92TC00482.

Gehrels, G.E., Rusmore, M., Woodsworth, G., Crawford, M., Andronicos, C., Hollister, L., Patchett, J., Ducea, M., Butler, R., Klepeis, K., and Davidson, C., 2009, U-Th-Pb geochronology of the Coast Mountains batholith in north-coastal British Columbia: Constraints on age and tectonic

evolution: Geological Society of America Bulletin, v. 121, no. 9–10, p. 1341–1361, https://doi.org/10.1130/B26404.1.

George, S.W.M., Nelson, J.L., Alberts, D., Greig, C.J., and Gehrels, G.E., 2021, Triassic–Jurassic accretionary history and tectonic origin of Stikinia from U-Pb geochronology and Lu-Hf isotope analysis, British Columbia: Tectonics, v. 40, no. 4, https://doi.org/10.1029/2020TC006505.

Green, T.H., and Pearson, N.J., 1987, An experimental study of Nb and Ta partitioning between Ti-rich minerals and silicate liquids at high pressure and temperature: Geochimica et Cosmochimica Acta, v. 51, no. 1, p. 55–62, https://doi.org/10.1016/0016-7037(87)90006-8.

Greenwood, H.J., Woodsworth, G.J., Read, P.B., Ghent, E.D., and Evenchick, C.A., 1991, Metamorphism, *in* Gabrielse, H., and Yorath, C.J., eds., Geology of the Cordilleran Orogen in Canada: Geological Survey of Canada, Geology of Canada 4, p. 533–570, https://doi.org/10.1130/DNAG-GNA-G2.533.

Gunning, M.H., Bamber, E.W., Brown, D.A., Rui, L., Mamet, B.L., and Orchard, M.J., 1994, The Permian Ambition Formation of Northwestern Stikinia, British Columbia, *in* Embry, A.F., Beauchamp, B., and Glass, D.J., eds., Pangea: Global Environments and Resources, Canadian Society of Petroleum Geologists, Memoir 17, p. 589–619.

Gunning, M.H., Hodder, R.W.H., and Nelson, J.L., 2006, Contrasting volcanic styles within the Paleozoic Stikine assemblage, western Stikine terrane, northwestern British Columbia, *in* Colpron, M., and Nelson, J.L., eds., Paleozoic Evolution and Metallogeny of Pericratonic Terranes at the Ancient Pacific Margin of North America, Canadian and Alaskan Cordillera: Geological Association of Canada Special Paper 45, p. 201–228.

Gunning, M.H., Fedorowski, J., Orchard, M.J., Bamber, E.W., Friedman, R., Rui, L., Anderson, R.G., Mamet, B.L., and Mortensen, J.K., 2007, The mid-Carboniferous Arctic Lake Formation, northwestern Stikine terrane, British Columbia: Bulletin of Canadian Petroleum Geology, v. 55, p. 21–50, https://doi.org/10.2113/gscpgbull.55.1.21.

Hadlari, T., Davis, W.J., Dewing, K., Heaman, L.M., Lemieux, Y., Ootes, L., Pratt, B.R., and Pyle, L.J., 2012, Two detrital zircon signatures for the Cambrian passive margin of northern Laurentia highlighted by new U-Pb results from northern Canada: Geological Society of America Bulletin, v. 124, no. 7–8, p. 1155–1168, https://doi.org/10.1130/B30530.1.

Harigane, Y., Michibayashi, K., and Ohara, Y., 2011, Relicts of deformed lithospheric mantle within serpentinites and weathered peridotites from the Godzilla megamullion, Parece Vela back-arc basin, Philippine Sea: The Island Arc, v. 20, no. 2, p. 174–187, https://doi.org/10.1111/j.1440-1738.2011.00759.x.

Hawkesworth, C., Turner, S., Gallagher, K., Hunter, A., Bradshaw, T., and Rogers, N., 1995, Calc-alkaline magmatism, lithospheric thinning and extension in the Basin and Range: Journal of Geophysical Research: Solid Earth, v. 100, no. B6, p. 10,271–10,286, https://doi.org/10.1029/94JB02508.

Herron, M.M., 1988, Geochemical classification of terrigenous sands and shales from core or log data: Journal of Sedimentary Research, v. 58, no. 5, p. 820–829, https://doi.org/10.1306/212F8E77-2B24-11D7-8648000102C1865D.

Hirahara, Y., Kimura, J.I., Senda, R., Miyazaki, T., Kawabata, H., Takahashi, T., Chang, Q., Vaglarov, B.S., Sato, T., and Kodaira, S., 2015, Geochemical variations in Japan Sea back-arc basin basalts formed by high-temperature adiabatic melting of mantle metasomatized by sediment subduction components: Geochemistry, Geophysics, Geosystems, v. 16, no. 5, p. 1324–1347, https://doi.org/10.1002/2015GC005720.

Hirata, N., Karp, B.Y., Yamaguchi, T., Kanazawa, T., Suyehiro, K., Kasahara, J., Shiobara, H., Shinohara, M., and Kinoshita, H., 1992, Oceanic crust in the Japan Basin of the Japan Sea by the 1990 Japan-USSR Expedition: Geophysical Research Letters, v. 19, no. 20, p. 2027–2030, https://doi.org/10.1029/92GL02094.

Hooper, P.R., Bailey, D.G., and Holder, G.M., 1995, Tertiary calc-alkaline magmatism associated with lithospheric extension in the Pacific Northwest: Journal of Geophysical Research: Solid Earth, v. 100, no. B6, p. 10,303–10,319, https://doi.org/10.1029/94JB03328.

Horstwood, M.S., Košler, J., Gehrels, G., Jackson, S.E., McLean, N.M., Paton, C., Pearson, N.J., Sircombe, K., Sylvester, P., Vermeesch, P., and Bowring, J.F., 2016, Community-derived standards for LA-ICP-MS U-(Th-) Pb geochronology—Uncertainty propagation, age interpretation and data reporting: Geostandards and Geoanalytical Research, v. 40, no. 3, p. 311–332, https://doi.org/10.1111/j.1751-908X.2016.00379.x.

Hoskin, P.W., and Schaltegger, U., 2003, The composition of zircon and igneous and metamorphic petrogenesis: Reviews in Mineralogy and Geochemistry, v. 53, no. 1, p. 27–62, https://doi.org/10.2113/0530027.

Huang, C.Y., Yuan, P.B., and Tsao, S.J., 2006, Temporal and spatial records of active arc-continent collision in Taiwan: A synthesis: Geological Society of America Bulletin, v. 118, no. 3–4, p. 274–288, https://doi.org/10.1130/B25527.1.

Huang, L., Geng, W., and Sun, Z.L., 2018, Origin of the serpentinites in the Lichi mélange, eastern Taiwan, China: Implication from petrology and geochronology: China Geology, v. 1, no. 4, p. 477–484, https://doi.org/10.31035/cg2018070.

Johnston, S.T., Canil, D., and Heaman, L.H., 2007, Permian exhumation of the Buffalo Pitts orogenic peridotite massif, northern Cordillera, Yukon: Canadian Journal of Earth Sciences, v. 44, no. 3, p. 275–286, https://doi.org/10.1139/e06-078.

Juan, V.C., Lo, H.J., and Chen, C.H., 1983, Geotectonics of Taiwan—An overview, *in* Hilde, T.W.C., and Uyeda, S., eds., Geodynamics of the Western Pacific–Indonesian Region: American Geophysical Union Geodynamics Monograph 11, p. 379–386, https://doi.org/10.1029/GD011p0379.

Kellett, D.A., and Iraheta Muniz, P., 2019, Detrital U-Pb Zircon and $^{40}Ar/^{39}Ar$ Muscovite Geochronology of the Whitehorse Trough, and Surrounding Rocks, Yukon and British Columbia: Geological Survey of Canada Open-File 8565, 35 p., https://doi.org/10.4095/314694.

Klein, E.M., 2004, Geochemistry of the igneous oceanic crust, *in* Holland, H.D., and Turekian, K.K., eds., Treatise on Geochemistry Volume 3: The Crust: Amsterdam, Netherlands, Elsevier, p. 433–463, https://doi.org/10.1016/B0-08-043751-6/03030-9.

Kroeger, E.D., McClelland, W.C., Colpron, M., Piercey, S.J., and Gehrels, G.E., 2023, Detrital zircon U-Pb and Hf isotope signature of Carboniferous and older strata of the Yukon-Tanana terrane in Yukon, Canadian Cordillera: Implications for terrane correlations and the onset of Late Devonian arc magmatism: Geosphere, v. 19, no. 4, p. 1032–1056, https://doi.org/10.1130/GES02607.1.

LaMaskin, T.A., 2012, Detrital zircon facies of Cordilleran terranes in western North America: GSA Today, v. 22, no. 3, p. 4–11, https://doi.org/10.1130/GSATG142A.1.

Lane, L.S., and Gehrels, G.E., 2014, Detrital zircon lineages of late Neoproterozoic and Cambrian strata, NW Laurentia: Geological Society of America Bulletin, v. 126, no. 3–4, p. 398–414, https://doi.org/10.1130/B30848.1.

Larson, K.P., Gervais, F., and Kellett, D.A., 2013, A *P-T-t-D* discontinuity in east-central Nepal: Implications for the evolution of the Himalayan mid-crust: Lithos, v. 179, p. 275–292, https://doi.org/10.1016/j.lithos.2013.08.012.

Leloup, P.H., Lacassin, R., Tapponnier, P., Schärer, U., Zhong, D., Liu, X., Zhang, L., Ji, S., and Trinh, P.T., 1995, The Ailao Shan–Red river shear zone (Yunnan, China), Tertiary transform boundary of Indochina: Tectonophysics, v. 251, no. 1–4, p. 3–84, https://doi.org/10.1016/0040-1951(95)00070-4.

Leslie, C.D., 2009, Detrital Zircon Geochronology and Rift-Related Magmatism: Central Mackenzie Mountains, Northwest Territories [M.Sc. thesis]: Vancouver, British Columbia, Canada, University of British Columbia, 224 p., https://doi.org/10.14288/1.0052744.

Logan, J.M., and Mihalynuk, M.G., 2014, Tectonic controls on early Mesozoic paired alkaline porphyry deposit belts (Cu-Au±Ag-Pt-Pd-Mo) within the Canadian Cordillera: Economic Geology, v. 109, p. 827–858, https://doi.org/10.2113/econgeo.109.4.827.

Logan, J.M., Drobe, J.R., and McClelland, W.C., 2000, Geology of the Forrest Kerr–Mess Creek Area, Northwestern British Columbia (NTS 104B/10, 15 & 104/G2 & 7W): British Columbia Ministry of Energy, Mines and Petroleum Resources, British Columbia Geological Survey Bulletin 104, 164 p.

Ludwig, K.R., 2003a, User's Manual for Isoplot/Ex Rev. 3.00: A Geochronological Toolkit for Microsoft Excel: Berkeley Geochronology Center Special Publication 4, 70 p.

Ludwig, K.R., 2003b, Mathematical-statistical treatment of data and errors for $^{230}Th/U$ geochronology: Reviews in Mineralogy and Geochemistry, v. 52, no. 1, p. 631–656, https://doi.org/10.2113/0520631.

MacLeod, C.J., Searle, R.C., Murton, B.J., Casey, J.F., Mallows, C., Unsworth, S.C., Achenbach, K.L., and Harris, M., 2009, Life cycle of oceanic core complexes: Earth and Planetary Science Letters, v. 287, no. 3–4, p. 333–344, https://doi.org/10.1016/j.epsl.2009.08.016.

Matthews, W., Guest, B., and Madronich, L., 2018, Latest Neoproterozoic to Cambrian detrital zircon facies of western Laurentia: Geosphere, v. 14, no. 1, p. 243–264, https://doi.org/10.1130/GES01544.1.

McClelland, W.C., Gehrels, G.E., Samson, S.D., and Patchett, P.J., 1992, Protolith relations of the Gravina belt and Yukon-Tanana terrane in central southeastern Alaska: The Journal of Geology, v. 100, no. 1, p. 107–123, https://doi.org/10.1086/629574.

McLennan, S.M., 2001, Relationships between the trace element composition of sedimentary rocks and upper continental crust: Geochemistry, Geophysics, Geosystems, v. 2, no. 4, 1021, https://doi.org/10.1029/2000GC000109.

Mihalynuk, M.G., and Mountjoy, K.J., 1990, Geology of the Tagish Lake area (104M/8, 9E), *in* British Columbia Ministry of Energy, Mines and Petroleum Resources Geological Fieldwork 1989: British Columbia Geological Survey Paper 1990–1, p. 181–196.

Mihalynuk, M.G., and Rouse, J.N., 1988, Preliminary geology of the Tutshi Lake area, northwestern British Columbia (104M/15), *in* British Columbia Ministry of Energy, Mines and Petroleum Resources Geological Fieldwork 1987: British Columbia Geological Survey Paper 1988–1, p. 217–231.

Mihalynuk, M.G., Currie, L.D., and Arksey, R.L., 1989, The geology of the Tagish Lake area (Fantail Lake and Warm Creek, 104M/9W and 10E), *in* British Columbia Ministry of Energy, Mines and Petroleum Resources Geological Fieldwork 1988: British Columbia Geological Survey Paper 1989–1, p. 293–310.

Mihalynuk, M.G., Smith, M.T., Hancock, K.D., and Dudka, S., 1994, Regional and economic geology of the Tulsequah River and Glacier areas (104K/12 & 13), *in* British Columbia Ministry of Energy, Mines and Petroleum Resources Geological Fieldwork 1993: British Columbia Geological Survey Paper 1994–1, p. 171–197.

Mihalynuk, M.G., Mountjoy, K.J., Smith, M.T., Currie, L.D., Gabites, J.E., Tipper, H.W., Orchard, M.J., Poulton, T.P., and Cordey, F., 1999, Geology and Mineral Resources of the Tagish Lake Area (NTS 104M/8, 9, 10E, 15 and 104N/12W), Northwestern British Columbia: British Columbia Ministry of Energy and Mines Bulletin 105, 217 p.

Mihalynuk, M.G., Friedman, R.M., Devine, F., Heaman, L.M., Colpron, M., and Nelson, J.L., 2006, Protolith age and deformation history of the Big Salmon complex, relicts of a Paleozoic continental arc in northern British Columbia, *in* Colpron, M., and Nelson, J.L., eds., Paleozoic Evolution and Metallogeny of Pericratonic Terranes at the Ancient Pacific Margin of North America, Canadian and Alaskan Cordillera: Geological Association of Canada Special Paper 45, p. 179–200.

Miller, J.S., Matzel, J.E., Miller, C.F., Burgess, S.D., and Miller, R.B., 2007, Zircon growth and recycling during the assembly of large, composite arc plutons: Journal of Volcanology and Geothermal Research, v. 167, no. 1–4, p. 282–299, https://doi.org/10.1016/j.jvolgeores.2007.04.019.

Monger, J.W.H., and Gibson, H.D., 2019, Mesozoic–Cenozoic deformation in the Canadian Cordillera: The record of a "continental bulldozer"?: Tectonophysics, v. 757, p. 153–169, https://doi.org/10.1016/j.tecto.2018.12.023.

Monger, J.W.H., Price, R.A., and Tempelman-Kluit, D.J., 1982, Tectonic accretion and the origin of the two major metamorphic and plutonic welts in the Canadian Cordillera: Geology, v. 10, no. 2, p. 70–75, https://doi.org/10.1130/0091-7613(1982)10<70:TAATOO>2.0.CO;2.

Monger, J.W.H., Van der Heyden, P., Journeay, J.M., Evenchick, C.A., and Mahoney, J.B., 1994, Jurassic–Cretaceous basins along the Canadian Coast belt: Their bearing on pre–mid-Cretaceous sinistral displacements: Geology, v. 22, no. 2, p. 175–178, https://doi.org/10.1130/0091-7613(1994)022<0175:JCBATC>2.3.CO;2.

Mortensen, J.K., 1992, Pre–mid-Mesozoic tectonic evolution of the Yukon-Tanana terrane, Yukon and Alaska: Tectonics, v. 11, no. 4, p. 836–853, https://doi.org/10.1029/91TC01169.

Murphy, D.C., Mortensen, J.K., Piercey, S.J., Orchard, M.J., Gehrels, G.E., Colpron, M., and Nelson, J.L., 2006, Mid-Paleozoic to early Mesozoic tectonostratigraphic evolution of Yukon-Tanana and Slide Mountain terranes and affiliated overlap assemblages, Finlayson Lake massive sulphide district, southeastern Yukon, *in* Colpron, M., and Nelson, J.L., eds., Paleozoic Evolution and Metallogeny of Pericratonic Terranes at the Ancient Pacific Margin of North America, Canadian and Alaskan Cordillera: Geological Association of Canada Special Paper 45, p. 75–105.

Natural Resources Canada, 2016, Canadian Digital Elevation Model, 1945–2011, https://open.canada.ca/data/en/dataset/7f245e4d-76c2-4caa-951a-45d1d2051333 (accessed March 2018).

Nelson, J.L., 1993, The Sylvester allochthon: Upper Paleozoic marginal-basin and island-arc terranes in northern British Columbia: Canadian Journal of Earth Sciences, v. 30, no. 3, p. 631–643, https://doi.org/10.1139/e93-048.

Nelson, J.L., 2017, Composite pericratonic basement of west-central Stikinia and its influence on Jurassic magma conduits: Examples from the Terrace-Ecstall and Anyox areas, *in* British Columbia Ministry of Energy, Mines and Petroleum Resources Geological Fieldwork 2016: British Columbia Geological Survey Paper 2017–1, p. 61–82.

Nelson, J.L., and Friedman, R., 2004, Superimposed Quesnel (late Paleozoic–Jurassic) and Yukon–Tanana (Devonian–Mississippian) arc assemblages, Cassiar Mountains, northern British Columbia: Field, U-Pb, and igneous petrochemical evidence: Canadian Journal of Earth Sciences, v. 41, no. 10, p. 1201–1235, https://doi.org/10.1139/e04-028.

Nelson, J.L., Colpron, M., Piercey, S.J., Dusel-Bacon, C., Murphy, D.C., and Roots, C.F., 2006, Paleozoic tectonic and metallogenetic evolution of pericratonic terranes in Yukon, northern British Columbia and eastern Alaska, *in* Colpron, M., and Nelson, J.L., eds., Paleozoic Evolution and Metallogeny of Pericratonic Terranes at the Ancient Pacific Margin of North America, Canadian and Alaskan Cordillera: Geological Association of Canada Special Paper 45, p. 323–360.

Nelson, J.L., Colpron, M., and Israel, S., 2013, The Cordillera of British Columbia, Yukon, and Alaska: Tectonics and metallogeny, *in* Colpron, M., Bissig, T., Rusk, B.G., and Thompson, J.F.H., eds., Tectonics, Metallogeny, and Discovery: The North American Cordillera and Similar Accretionary Settings: Society of Economic Geologists Special Publication 17, p. 53–109, https://doi.org/10.5382/SP.17.03.

Nelson, J.L., van Straaten, B., and Friedman, R., 2022, Latest Triassic–Early Jurassic Stikine–Yukon-Tanana terrane collision and the onset of accretion in the Canadian Cordillera: Insights from Hazelton Group detrital zircon provenance and arc–back-arc configuration: Geosphere, v. 18, no. 2, p. 670–696, https://doi.org/10.1130/GES02444.1.

Ootes, L., Castonguay, S., Friedman, R., Devine, F., and Simmonds, R., 2018, Testing the relationship between the Llewellyn fault, Tally-Ho shear zone, and gold mineralization in northwest British Columbia, *in* British Columbia Ministry of Energy, Mines and Petroleum Resources Geological Fieldwork 2017: British Columbia Geological Survey Paper 2018–1, p. 67–81.

Ootes, L., Castonguay, S., Friedman, R., and Devine, F., 2019, Superimposed auriferous structural events along the Llewellyn–Tally Ho deformation corridor in southern Yukon and northwest British Columbia, *in* Rogers, N., ed., Targeted Geoscience Initiative: 2018 Report of Activities: Geological Survey of Canada Open-File 8549, p. 49–58, https://doi.org/10.4095/313636.

Ootes, L., Milidragovic, D., Friedman, R., Wall, C., Cordey, F., Luo, Y., Jones, G., Pearson, D.G., and Bergen, A., 2022, A juvenile Paleozoic ocean floor origin for eastern Stikinia, Canadian Cordillera: Geosphere, v. 18, no. 4, p. 1297–1315, https://doi.org/10.1130/GES02459.1.

Park, S.H., Michael, P.J., Kamenov, G.D., Lee, S.M., Hauff, F., and Lee, K.Y., 2018, Petrogenesis of basalts along the eastern Woodlark spreading center, equatorial western Pacific: Lithos, v. 316, p. 122–136, https://doi.org/10.1016/j.lithos.2018.07.003.

Parsons, A.J., Coleman, M.J., Ryan, J.J., Zagorevski, A., Joyce, N.L., Gibson, H.D., and Larson, K.P., 2018, Structural evolution of a crustal-scale shear zone through a decreasing temperature regime: The Yukon River shear zone, Yukon-Tanana terrane, northern Cordillera: Lithosphere, v. 10, no. 6, p. 760–782, https://doi.org/10.1130/L724.1.

Parsons, A.J., Zagorevski, A., Ryan, J.J., McClelland, W.C., Van Staal, C.R., Coleman, M.J., and Golding, M.L., 2019, Petrogenesis of the Dunite Peak ophiolite, south-central Yukon, and the distinction between upper-plate and lower-plate settings: A new hypothesis for the late Paleozoic–early Mesozoic tectonic evolution of the northern Cordillera: Geological Society of America Bulletin, v. 131, no. 1–2, p. 274–298, https://doi.org/10.1130/B31964.1.

Parsons, A.J., McClelland, W.C., Zagorevski, A., Ryan, J.J., Coleman, M.J., Cleven, N., and van Staal, C.R., 2022, U-Pb zircon geochronology from the northern Cordillera, central Yukon, with implications for its tectonic assembly: Tectonics, v. 41, no. 2, https://doi.org/10.1029/2021TC006918.

Pearce, J.A., 1996, A user's guide to basalt discrimination diagrams, *in* Wyman, D.A., ed., Trace Element Geochemistry of Volcanic Rocks: Applications for Massive Sulphide Exploration: Geological Association of Canada Short Course Notes 12, p. 79–113.

Pearce, J.A., 2008, Geochemical fingerprinting of oceanic basalts with applications to ophiolite classification and the search for Archean oceanic crust: Lithos, v. 100, no. 1–4, p. 14–48, https://doi.org/10.1016/j.lithos.2007.06.016.

Pearce, J.A., 2014, Immobile element fingerprinting of ophiolites: Elements, v. 10, no. 2, p. 101–108, https://doi.org/10.2113/gselements.10.2.101.

Pearce, J.A., Harris, N.B., and Tindle, A.G., 1984, Trace element discrimination diagrams for the tectonic interpretation of granitic rocks: Journal of Petrology, v. 25, no. 4, p. 956–983, https://doi.org/10.1093/petrology/25.4.956.

Pecha, M.E., Gehrels, G.E., McClelland, W.C., Giesler, D., White, C., and Yokelson, I., 2016, Detrital zircon U-Pb geochronology and Hf isotope geochemistry of the Yukon-Tanana terrane, Coast Mountains, southeast Alaska: Geosphere, v. 12, no. 5, p. 1556–1574, https://doi.org/10.1130/GES01303.1.

Perfit, M.R., Langmuir, C.H., Backisapa, M., Chappell, B., Johnson, R.W., Staudigel, H., and Taylor, S.R., 1987, Geochemistry and petrology of volcanic rocks from the Woodlark Basin: Addressing questions of ridge subduction, *in* Taylor, B., and Exon, J.L., eds., Marine Geology, Geophysics and Geochemistry of the Woodlark Basin–Solomon Islands: Houston, Texas, Circum-Pacific Council for Energy and Mineral Resources, Circum-Pacific Earth Sciences Series 7, p. 113–154.

Petrie, M.B., Massonne, H.J., Gilotti, J.A., McClelland, W.C., and Van Staal, C., 2016, The *P-T* path of eclogites in the St. Cyr klippe, Yukon, Canada: Permian metamorphism of a coherent high-pressure unit in an accreted terrane of the North American Cordillera: European Journal of Mineralogy, v. 28, no. 6, p. 1111–1130, https://doi.org/10.1127/ejm/2016/0028-2576.

Petterson, M.G., Haldane, M.I., Smith, D.J., Billy, D., and Jordan, N.J., 2011, Geochemistry and petrogenesis of the Gallego volcanic field, Solomon Islands, SW Pacific, and geotectonic implications: Lithos, v. 125, no. 3–4, p. 915–927, https://doi.org/10.1016/j.lithos.2011.05.008.

Philippot, P., Blichert-Toft, J., Perchuk, A., Costa, S., and Gerasimov, V., 2001, Lu-Hf and Ar-Ar chronometry supports extreme rate of subduction zone metamorphism deduced from geospeedometry: Tectonophysics, v. 342, no. 1–2, p. 23–38, https://doi.org/10.1016/S0040-1951(01)00155-X.

Piercey, S.J., and Colpron, M., 2009, Composition and provenance of the Snowcap assemblage, basement to the Yukon-Tanana terrane, northern Cordillera: Implications for Cordilleran crustal growth: Geosphere, v. 5, no. 5, p. 439–464, https://doi.org/10.1130/GES00505.S3.

Piercey, S.J., Mortensen, J.K., Murphy, D.C., Paradis, S., and Creaser, R.A., 2002, Geochemistry and tectonic significance of alkalic mafic magmatism in the Yukon-Tanana terrane, Finlayson Lake region, Yukon: Canadian Journal of Earth Sciences, v. 39, no. 12, p. 1729–1744, https://doi.org/10.1139/e02-090.

Piercey, S.J., Murphy, D.C., Mortensen, J.K., and Creaser, R.A., 2004, Mid-Paleozoic initiation of the northern Cordilleran marginal backarc basin: Geologic, geochemical, and neodymium isotope evidence from the oldest mafic magmatic rocks in the Yukon-Tanana terrane, Finlayson Lake district, southeast Yukon, Canada: Geological Society of America Bulletin, v. 116, no. 9–10, p. 1087–1106, https://doi.org/10.1130/B25162.1.

Piercey, S.J., Nelson, J.L., Colpron, M., Dusel-Bacon, C., Simard, R.L., and Roots, C.F., 2006, Paleozoic magmatism and crustal recycling along the ancient Pacific margin of North America, northern Cordillera, *in* Colpron, M., and Nelson, J.L., eds., Paleozoic Evolution and Metallogeny of Pericratonic Terranes at the Ancient Pacific Margin of North America, Canadian and Alaskan Cordillera: Geological Association of Canada Special Paper 45, p. 281–322.

Pouclet, A., Lee, J.S., Vidal, P., Cousens, B., and Bellon, H., 1994, Cretaceous to Cenozoic volcanism in South Korea and in the Sea of Japan: Magmatic constraints on the opening of the back-arc basin, *in* Smellie, J.L., ed., Volcanism Associated with Extension at Consuming Plate Margins: Geological Society, London, Special Publication 81, p. 169–191, https://doi.org/10.1144/GSL.SP.1994.081.01.10.

Reagan, M.K., Heaton, D.E., Schmitz, M.D., Pearce, J.A., Shervais, J.W., and Koppers, A.A., 2019, Forearc ages reveal extensive short-lived and rapid seafloor spreading following subduction initiation: Earth and Planetary Science Letters, v. 506, p. 520–529, https://doi.org/10.1016/j.epsl.2018.11.020.

Richards, J.P., Chappell, B.W., and McCulloch, M.T., 1990, Intraplate-type magmatism in a continent–island-arc collision zone: Porgera intrusive complex, Papua New Guinea: Geology, v. 18, no. 10, p. 958–961, https://doi.org/10.1130/0091-7613(1990)018<0958:ITMIAC>2.3.CO;2.

Rivers, T., Culshaw, N., Hynes, A., Indares, A., Jamieson, R., Martignole, J., Percival, J.A., Cook, F.A., and Clowes, R.M., 2012, The Grenville orogen—A post-LITHOPROBE perspective, *in* Percival, J.A., Cook, F.A., and Clowes, R.M., eds., Tectonic Styles in Canada: The Lithoprobe Perspective: Geological Association of Canada Special Paper 49, p. 97–238.

Robertson, A.H.F., 2007, Evidence of continental breakup from the Newfoundland rifted margin (Ocean Drilling Program Leg 210): Lower Cretaceous seafloor formed by exhumation of subcontinental mantle lithosphere, and the transition to seafloor spreading, *in* Tucholke, B.E., Sibuet, J.-C., and Klaus, A., eds., Proceedings of the Ocean Drilling Program, Scientific Results, Volume 210: College Station, Texas, Ocean Drilling Program, p. 1–69, https://doi.org/10.2973/odp.proc.sr.210.104.2007.

Rubatto, D., 2017, Zircon: The metamorphic mineral: Reviews in Mineralogy and Geochemistry, v. 83, no. 1, p. 261–295, https://doi.org/10.2138/rmg.2017.83.9.

Rubatto, D., and Gebauer, D., 2000, Use of cathodoluminescence for U-Pb zircon dating by ion microprobe: Some examples from the western Alps, *in* Pagel, M., Barbin, V., Blanc, P., and Ohnenstetter, D., eds., Cathodoluminescence in Geosciences: Berlin, Springer, p. 373–400, https://doi.org/10.1007/978-3-662-04086-7_15.

Ryan, J.J., Zagorevski, A., Williams, S.P., Roots, C., Ciolkiewics, W., Hayward, N., and Chapman, J.B., 2013, Geology, Stevenson Ridge (Northwest Part), Yukon: Geological Survey of Canada Canadian Geoscience Map 117, scale 1:100,000, https://doi.org/10.4095/292408.

Ryan, J.J., Zagorevski, A., Roots, C.F., and Joyce, N., 2014, Paleozoic Tectonostratigraphy of the Northern Stevenson Ridge Area, Yukon: Geological Survey of Canada Current Research 2014–4, p. 1–13, https://doi.org/10.4095/293924.

Ryan, J.J., Zagorevski, A., Cleven, N.R., Parsons, A.J., and Joyce, N.L., 2021, Architecture of pericratonic Yukon-Tanana terrane in the northern Cordillera, *in* Ryan, J.J., and Zagorevski, A., eds., Northern Cordillera Geology: A Synthesis of Research from the Geo-Mapping for Energy and Minerals Program, British Columbia and Yukon: Geological Survey of Canada Bulletin 610, p. 67–93, https://doi.org/10.4095/326062.

Ryan, W.B., Carbotte, S.M., Coplan, J.O., O'Hara, S., Melkonian, A., Arko, R., Weissel, R.A., Ferrini, V., Goodwillie, A., Nitsche, F., and Bonczkowski, J., 2009, Global multi-resolution topography synthesis: Geochemistry, Geophysics, Geosystems, v. 10, no. 3, Q03014, https://doi.org/10.1029/2008GC002332.

Sack, P.J., Colpron, M., Crowley, J.L., Ryan, J.J., Allan, M.M., Beranek, L.P., Joyce, N.L., Mortensen, J.K., Israel, S., and Chapman, J.B., 2020, Atlas of Late Triassic to Jurassic Plutons in the Intermontane Terranes of Yukon: Yukon Geological Survey Open-File 2020–1, 365 p.

Saleeby, J.B., 1983, Accretionary tectonics of the North American Cordillera: Annual Review of Earth and Planetary Sciences, v. 11, p. 45–73, https://doi.org/10.1146/annurev.ea.11.050183.000401.

Saleeby, J.B., 2000, Geochronologic investigations along the Alexander-Taku terrane boundary, southern Revillagigedo Island to Cape Fox areas, southeast Alaska, *in* Stowell, H.H., and McClelland, W.C., eds., Tectonics of the Coast Mountains in SE Alaska and Coastal British Columbia: Geological Society of America Special Paper 343, p. 107–144, https://doi.org/10.1130/0-8137-2343-4.107.

Simard, R.L., Dostal, J., and Colpron, M., 2007, Rifting of a Mississippian continental arc system: Little Salmon formation, Yukon-Tanana terrane, northern Canadian Cordillera: Canadian Journal of Earth Sciences, v. 44, no. 9, p. 1267–1289, https://doi.org/10.1139/e07-022.

Sircombe, K.N., 2004, AgeDisplay: An EXCEL workbook to evaluate and display univariate geochronological data using binned frequency histograms and probability density distributions: Computers & Geosciences, v. 30, no. 1, p. 21–31, https://doi.org/10.1016/j.cageo.2003.09.006.

Soucy La Roche, R., Dyer, S.C., Zagorevski, A., Cottle, J.M., and Gaidies, F., 2022a, 150 Myr of episodic metamorphism recorded in the Yukon-Tanana terrane, northern Canadian Cordillera: Evidence from monazite and xenotime petrochronology: Lithosphere, v. 2022, no. 1, https://doi.org/10.2113/2022/7708357.

Soucy La Roche, R., Zagorevski, A., and Joyce, N., 2022b, Decrypting polyphase deformation with quartz crystallographic fabrics in the Wann River shear zone, northern Canadian Cordillera: Geological Society of America Abstracts with Programs, v. 54, no. 5, paper 147-4, https://doi.org/10.1130/abs/2022AM-380764.

Staples, R.D., Murphy, D.C., Gibson, H.D., Colpron, M., Berman, R.G., and Ryan, J.J., 2014, Middle Jurassic to earliest Cretaceous mid-crustal tectono-metamorphism in the northern Canadian Cordillera: Recording foreland-directed migration of an orogenic front: Geological Society of America Bulletin, v. 126, no. 11–12, p. 1511–1530, https://doi.org/10.1130/B31037.1.

Stern, R.A., 1997, The GSC Sensitive High Resolution Ion Microprobe (SHRIMP): Analytical techniques of zircon U-Th-Pb age determinations and performance evaluation, *in* Radiogenic Age and Isotopic Studies, Report 10: Geological Survey of Canada Current Research 1997-F, p. 1–31, https://doi.org/10.4095/209089.

Stern, R.A., and Amelin, Y., 2003, Assessment of errors in SIMS zircon U-Pb geochronology using a natural zircon standard and NIST SRM 610 glass: Chemical Geology, v. 197, no. 1–4, p. 111–142, https://doi.org/10.1016/S0009-2541(02)00320-0.

Stolz, A.J., Davies, G.R., Crawford, A.J., and Smith, I.M., 1993, Sr, Nd and Pb isotopic composition of calc-alkaline and peralkaline silicic volcanics from the D'Entrecasteaux Islands, Papua New Guinea, and their tectonic significance: Mineralogy and Petrology, v. 47, p. 103–126, https://doi.org/10.1007/BF01161562.

Sun, S.S., and McDonough, W.F., 1989, Chemical and isotopic systematics of oceanic basalts: Implications for mantle composition and processes, *in* Saunders, A.D., and Norry, M.J., eds., Magmatism in the Ocean Basins: Geological Society, London, Special Publication 42, p. 313–345, https://doi.org/10.1144/GSL.SP.1989.042.01.19.

Taira, A., 2001, Tectonic evolution of the Japanese island arc system: Annual Review of Earth and Planetary Sciences, v. 29, no. 1, p. 109–134, https://doi.org/10.1146/annurev.earth.29.1.109.

Tapponnier, P., Peltzer, G., Le Dain, A.Y., Armijo, R., and Cobbold, P., 1982, Propagating extrusion tectonics in Asia: New insights from simple experiments with plasticine: Geology, v. 10, no. 12, p. 611–616, https://doi.org/10.1130/0091-7613(1982)10<611:PETIAN>2.0.CO;2.

Taylor, B., and Hayes, D.E., 1980, The tectonic evolution of the South China Basin, *in* Hayes, D.E., ed., The Tectonic and Geologic Evolution of Southeast Asian Seas and Islands: American Geophysical Union Geophysical Monograph 23, p. 89–104, https://doi.org/10.1029/GM023p0089.

Taylor, S.R., and McLennan, S.M., 1985, The Continental Crust: Its Composition and Evolution: Oxford, UK, Blackwell Scientific Publications, 312 p.

Tempelman-Kluit, D.J., 1979, Transported cataclasite, ophiolite and granodiorite in Yukon: Evidence of arc-continent collision: Geological Survey of Canada Paper 79–14, p. 1–27, https://doi.org/10.4095/105928.

Tochilin, C.J., Gehrels, G.E., Nelson, J., and Mahoney, J.B., 2014, U-Pb and Hf isotope analysis of detrital zircons from the Banks Island assemblage (coastal British Columbia) and southern

Alexander terrane (southeast Alaska): Lithosphere, v. 6, no. 3, p. 200–215, https://doi.org/10.1130/L338.1.

Van Horne, A., Sato, H., and Ishiyama, T., 2017, Evolution of the Sea of Japan back-arc and some unsolved issues: Tectonophysics, v. 710, p. 6–20, https://doi.org/10.1016/j.tecto.2016.08.020.

van Staal, C.R., Zagorevski, A., McClelland, W.C., Escayola, M.P., Ryan, J.J., Parsons, A.J., and Proenza, J., 2018, Age and setting of Permian Slide Mountain terrane ophiolitic ultramafic-mafic complexes in the Yukon: Implications for late Paleozoic–early Mesozoic tectonic models in the northern Canadian Cordillera: Tectonophysics, v. 744, p. 458–483, https://doi.org/10.1016/j.tecto.2018.07.008.

Vice, L., Gibson, H.D., and Israel, S., 2020, Late Cretaceous to Paleocene tectonometamorphic evolution of the Blanchard River assemblage, southwest Yukon: New insight into the terminal accretion of insular terranes in the northern Cordillera: Lithosphere, v. 2020, no. 1, https://doi.org/10.2113/2020/2298288.

Walker, J.D., and Geissman, J.W., compilers, 2022, Geologic Time Scale v. 6.0: Boulder, Colorado, Geological Society of America, 1 p., https://doi.org/10.1130/2022.CTS006C.

Weissel, J.K., Taylor, B., and Karner, G.D., 1982, The opening of the Woodlark Basin, subduction of the Woodlark spreading system, and the evolution of northern Melanesia since mid-Pliocene time: Tectonophysics, v. 87, no. 1–4, p. 253–277, https://doi.org/10.1016/0040-1951(82)90229-3.

Wendt, I., and Carl, C., 1991, The statistical distribution of the mean squared weighted deviation: Chemical Geology: Isotope Geoscience Section, v. 86, no. 4, p. 275–285, https://doi.org/10.1016/0168-9622(91)90010-T.

Wheeler, J.O., Brookfield, A.J., Gabrielse, H., Monger, J.W.H., Tipper, H.W., and Woodsworth, G.J., 1991, Terrane Map of the Canadian Cordillera: Geological Survey of Canada "A" Series Map 1713A, scale 1:2,000,000, https://doi.org/10.4095/133550.

Whitmeyer, S.J., and Karlstrom, K.E., 2007, Tectonic model for the Proterozoic growth of North America: Geosphere, v. 3, no. 4, p. 220–259, https://doi.org/10.1130/GES00055.1.

Woodhead, J.D., and Johnson, R.W., 1993, Isotopic and trace-element profiles across the New Britain island arc, Papua New Guinea: Contributions to Mineralogy and Petrology, v. 113, no. 4, p. 479–491, https://doi.org/10.1007/BF00698317.

Yan, P., Deng, H., Liu, H., Zhang, Z., and Jiang, Y., 2006, The temporal and spatial distribution of volcanism in the South China Sea region: Journal of Asian Earth Sciences, v. 27, no. 5, p. 647–659, https://doi.org/10.1016/j.jseaes.2005.06.005.

Yokelson, I., Gehrels, G.E., Pecha, M., Giesler, D., White, C., and McClelland, W.C., 2015, U-Pb and Hf isotope analysis of detrital zircons from Mesozoic strata of the Gravina belt, southeast Alaska: Tectonics, v. 34, no. 10, p. 2052–2066, https://doi.org/10.1002/2015TC003955.

Yonkee, W.A., Dehler, C.D., Link, P.K., Balgord, E.A., Keeley, J.A., Hayes, D.S., Wells, M.L., Fanning, C.M., and Johnston, S.M., 2014, Tectono-stratigraphic framework of Neoproterozoic to Cambrian strata, west-central US: Protracted rifting, glaciation, and evolution of the North American Cordilleran margin: Earth-Science Reviews, v. 136, p. 59–95, https://doi.org/10.1016/j.earscirev.2014.05.004.

Yoshida, T., Kimura, J.I., Yamada, R., Acocella, V., Sato, H., Zhao, D., Nakajima, J., Hasegawa, A., Okada, T., Honda, S., and Ishikawa, M., 2014, Evolution of late Cenozoic magmatism and the crust-mantle structure in the NE Japan arc, *in* Gómez-Tuena, A., Straub, S.M., and Zellmer, G.F., eds., Orogenic Andesites and Crustal Growth: Geological Society, London, Special Publication 385, p. 335–387, https://doi.org/10.1144/SP385.15.

Young, G.M., Jefferson, C.W., Delaney, G.D., and Yeo, G.M., 1979, Middle and late Proterozoic evolution of the northern Canadian Cordillera and Shield: Geology, v. 7, no. 3, p. 125–128, https://doi.org/10.1130/0091-7613(1979)7<125:MALPEO>2.0.CO;2.

Zagorevski, A., 2016, Geochemical Data of the Northern Cache Creek and Stikine Terranes and Their Overlap Assemblages, British Columbia and Yukon: Geological Survey of Canada Open-File 8039, 13 p., 1 zip file (superseded by Zagorevski, 2018).

Zagorevski, A., 2018, Geochemical Data of the Northern Cache Creek, Slide Mountain, and Stikine Terranes and Their Overlap Assemblages, British Columbia and Yukon: Geological Survey of Canada Open-File 8395, 12 p., 1 zip file.

Zagorevski, A., and van Staal, C.R., 2021, Cordilleran magmatism in Yukon and northern British Columbia: Characteristics, temporal variations and significance for the tectonic evolution of the northern Cordillera, *in* Ryan, J.J., and Zagorevski, A., eds., Northern Cordillera Geology: A Synthesis of Research from the Geo-Mapping for Energy and Minerals Program, British Columbia and Yukon: Geological Survey of Canada Bulletin 610, p. 95–122, https://doi.org/10.4095/326063.

Zagorevski, A., Soucy La Roche, R., Golding, M., Joyce, N., Regis, D., and Coleman, M., 2018, Stikinia Bedrock, British Columbia and Yukon, GEM-2 Cordillera Project, Report of Activities 2018: Geological Survey of Canada Open-File 8485, 12 p., https://doi.org/10.4095/311325.

Zagorevski, A., Bédard, J.H., Bogatu, A., Canil, D., Coleman, M., Golding, M., Joyce, N., Lawley, C., McGoldrick, S., Mihalynuk, M., Parsons, A., Schiarizza, P., and van Staal, C.R., 2021, Overview of Cordilleran oceanic terranes and their significance for the tectonic evolution of the northern Cordillera, *in* Ryan, J.J., and Zagorevski, A., eds., Northern Cordillera Geology: A Synthesis of Research from the Geo-Mapping for Energy and Minerals Program, British Columbia and Yukon: Geological Survey of Canada Bulletin 610, p. 21–65, https://doi.org/10.4095/326053.